Icarus **144**, 329–352 (2000)
doi:10.1006/icar.1999.6298, available online at http://www.idealibrary.com on IDEAL®

North Polar Region Craterforms on Mars: Geometric Characteristics from the Mars Orbiter Laser Altimeter

James B. Garvin

NASA–Goddard Space Flight Center, Geodynamics, Code 921, Greenbelt, Maryland 20771
E-mail: garvin@denali.gsfc.nasa.gov

Susan E. H. Sakimoto

USRA at NASA–Goddard Space Flight Center, Code 921, Greenbelt, Maryland 20771

James J. Frawley

Herring Bay Geophysics, Raytheon-STX, at NASA–Goddard Space Flight Center, Code 921, Greenbelt, Maryland 20771

and

Charles Schnetzler

SSAI at NASA–Goddard Space Flight Center, Code 920, Greenbelt, Maryland 20771

Received February 15, 1999; revised September 20, 1999

This study focuses on topographic characterization of ice-associated north polar region impact craters and several enigmatic polar craterforms using new information from the Mars Orbiter Laser Altimeter (MOLA), an instrument aboard the Mars Global Surveyor (MGS) orbiter. We find that, for ice-associated craters, the topography reveals several surprising results not previously apparent from orbital images alone. First, geometric properties for several impact craters associated with ice and frost deposits suggest that cavity infill is as high as 80% of reconstructed, preerosion levels. Second, craters associated with ice also demonstrate unique cavity geometries relative to their nonpolar counterparts. Finally, in some cases, ice-associated impact features are anomalously deep, on the basis of depths modeled from the best available scaling laws. We suggest that burial of these impact features by either episodic advance of the polar cap margin or by continuous deposition at the highest rates previously estimated for the north polar region of Mars has occurred. Subsequent stripping has exhumed the features, leaving behind cavity infill deposits, and a few of these display topographic levels above the surrounding preimpact surface. In at least one case, cavity interior deposits show layering with a typical thickness of ∼10 m, suggesting episodic deposition and ablation of materials as in the polar layered terrain. In addition to ice-associated craters, we investigated the topography of several enigmatic polar craterforms. In particular, a few craterforms within ∼150 km of the permanent north polar cap appear to resemble simple, effusive lava shield volcanoes found on Earth. Their geometric properties cannot be reconciled with previous suggestions that they were manifestations of martian hydromagmatic processes (i.e., maar volcanism). MOLA's initial measurements of impact craters and other craterforms in the north polar latitudes of Mars support the concept of a geologically recent surface, with evidence of effusive volcanism and enhanced sedimentation. In addition, the measured impact crater depths for ice-associated craters suggest at least a few cases of enhanced excavation and thus a possibly weaker target relative to the typical northern hemisphere plains.

Key Words: **Mars; impact craters; polar processes; ejecta; volcanism.**

INTRODUCTION

The north polar region of Mars (57°–90°N) offers an opportunity to evaluate the relative importance of several geologic processes in the evolution of the martian surface, including hypervelocity impact cratering, volcanism, and erosion. In particular, the sedimentation history in this region can be assessed on the basis of the geometric properties of impact craters, as has been accomplished for the south polar region by Plaut *et al.* (1988). In addition to the readily apparent impact craters, there are numerous craterforms in the north polar region of enigmatic origin. Hodges and Moore (1994) attributed some of these craterforms to hydromagmatic processes, perhaps similar to the explosive interactions of groundwater with magma that on Earth leads to the formation of maar craters. Other, less well-defined craterforms are also observed in Viking Orbiter images around the perimeter of the permanent north polar cap. Their origin and evolution remains unclear.

Many of the best-preserved impact craters in the north polar region are associated with high-albedo deposits of ice and frost

0019-1035/00 $35.00

(Garvin *et al.* 1998). In several cases, these ice-associated craters appear to be infilled with frost or ice deposits to levels in excess of what existing polar sedimentation models would suggest (Howard *et al.* 1982, Thomas *et al.* 1992). In this preliminary assessment of north polar region craterforms, our intention is to constrain the formation and modification histories of such features in order to investigate the efficiency of sedimentation over the most recent epoch of martian geologic history. Our approach is to employ newly available topographic measurements from the Mars Orbiter Laser Altimeter (MOLA), an instrument currently in orbit around Mars as part of the payload on the Mars Global Surveyor (MGS) spacecraft, to characterize the geometric properties (e.g., Pike 1980b) of all craters for which adequate sampling was achieved. This permits assessment of formation mechanisms as well as modification (i.e., infilling, slope evolution) processes. Zuber *et al.* (1998) has described the MOLA observations pertaining to the north polar cap of Mars and Smith *et al.* (1998) have summarized in general the first northern hemisphere measurements by MOLA. Here we study the impact and possible volcanic crater population at high northern latitudes sampled thus far by MOLA, using the data acquired as part of the Science Phasing Orbit (SPO) operations of MGS during the Spring and Summer of 1998. Garvin and Frawley (1998) have provided an initial framework for comparison of nonpolar impact craters and their geometric properties to those sampled in the North Polar Region.

We first summarize the MOLA measurements used as the basis of this work: the polar region topographic measurements acquired for "ice-associated" craterforms prior to the main mapping mission. Next, we discuss the geometric measurements (depth/diameter, cavity volume, ejecta thickness, etc.) of cavity and ejecta characteristics for ice-associated craters. This is followed with images and topography for examples of the best-sampled ice-associated craters and a few enigmatic craterforms of potentially volcanic origin. The discussion section includes the implications of our results in light of current models for cratering (e.g., Strom *et al.* 1992, Melosh 1989, Barlow and Bradley 1990, Craddock *et al.* 1997) and sedimentation in the north polar region of Mars.

MOLA OBSERVATIONS

MOLA acquired 188 tracks of topographic data across the high northern latitudes of Mars between April and late July of 1998 (Zuber *et al.* 1998). In addition to sampling the heights of the permanent north polar cap, MOLA acquired cross sections for many of the major impact craters known to exist in this region, including more than a dozen craters between ~9 and 80 km in diameter. Figure 1 shows the locations of the craters and craterforms whose cavities were well-sampled by MOLA (topography across the center 20% of the cavity) during this period. Craters described in detail are designated by alphabetic letters, A–K, in Fig. 1. Here we treat circular, closed depressions of unknown origin as "craterforms," although we recognize that most are either volcanic- or impact-related (Hodges and Moore 1994, Wilson and Head 1994). Barlow and Bradley (1990) have given a summary of martian impact crater properties as measured from Viking image photomosaics. Because of the relatively poor quality of Viking era imaging of the north polar region, their extensive morphologic catalog does not include many of the ice-associated craters traversed by MOLA at latitudes north of 65°N. Previous studies of ice in the martian regolith (Squyres *et al.* 1992, Jankowski and Squyres 1993) do not treat the population of north polar region impact craters associated with ice or frost above 65°N. We have considered in detail the morphologic characteristics of such features from MOLA topographic cross sections. MOLA observations consist of center-of-mass referenced surface elevations for footprints ~150 m in diameter with submeter vertical precision spaced every 330 to 390 m along the nadir–ground track of the MGS spacecraft. Because of the high vertical precision of these data, subtle topographic and hence local slope variations associated with crater landforms can be measured and interpreted. For example, Garvin and Frawley (1998) were able to quantify the relief of ejecta ramparts with less than 10 m in vertical relief on the basis of MOLA data for impact features in the middle latitudes of the northern hemisphere of Mars.

We have developed a semiautomated measurement system for quantifying a broad suite of geometric craterform parameters in order to characterize properties relevant to crater formation and modification (Roddy 1977, Pike 1980a,b). Figure 2 shows some of the parameters that are routinely measured for each crater. Table I summarizes the parameters depicted in Fig. 2, as well as several additional measured parameters. Before detailed measurements of crater properties can be accomplished, each

TABLE I
Description of Geometric Parameters Measured from MOLA Cross Sections of Craterforms (Fig. 1)

Parameter	Significance
D	Rim crest diameter
d	Depth from rim crest to floor
H	Average height of rim crest above preimpact surface
d/D	Aspect ratio of crater cavity
h_r	Ejecta rampart height
h_{cp}	Central peak height
V_{cav}	Cavity volume from numerical integration of rim crest as defined in MOLA cross section
V_{ej}	Ejecta volume from rim crest to topographically defined edge of continuous ejecta blanket (numerical integration)
V_{ej}/V_{cav}	Ejecta to cavity volume ratio
n	Exponent of power law fit to cavity topography from $z = kx^n$, where x is horizontal distance. Cavity is conical for $n = 1$, paraboloid for $n = 2$, etc.
ETF	Exponent b from power law fit to ejecta topography, i.e., $t_e = k(x/R)^b$

Note. Other parameters indicated on Fig. 1 (ejecta and cavity wall slope) are not listed above.

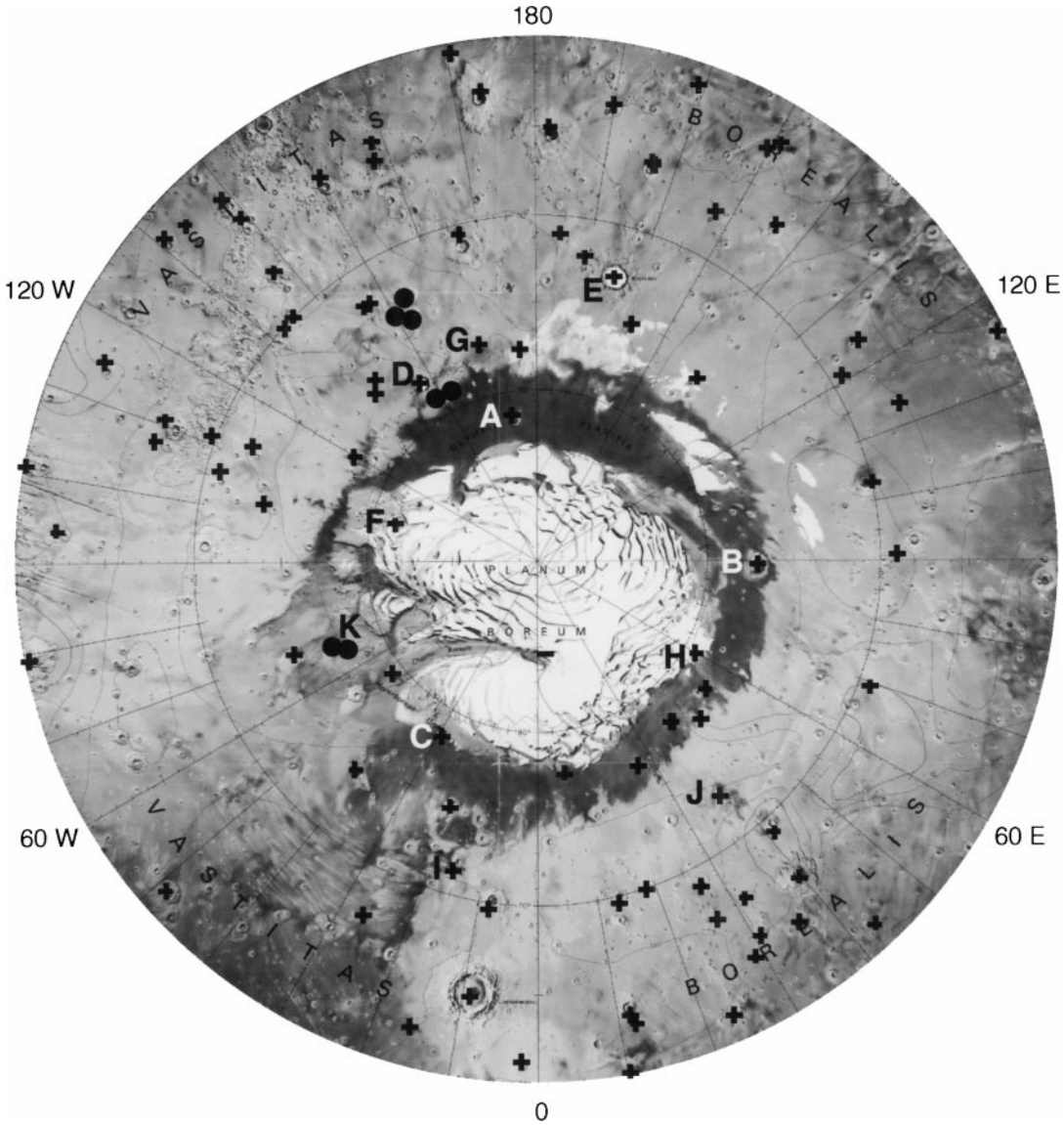

FIG. 1. Polar stereographic map of the northern polar region of Mars indicating crater locations (+'s are impact craters, filled circles are craterforms of possible volcanic origin). The latitude limit of the map is 60°N. Craters north of 70°N are the primary focus. Craters discussed in the text are designated by alphabetic characters (A–K). Crater A is illustrated in Fig. 3, Crater B in Fig. 4, etc.

MOLA profile must be compared with the highest available resolution Viking Mars Digital Image Mosaic (MDIM) image data in order to assess the actual position of the topographic cross section relative to the central axis of symmetry of the crater. This is necessary because of coordinate system disparities between the MGS MOLA data (areocentric coordinates) and the Viking MDIM (geographic coordinate frame). Smith *et al.* (1998) have discussed this issue, which often requires horizontal shifts of the MDIM so that the MOLA profile is registered properly to specific geographic features that it traverses. We believe that after shifting the MDIM image data relative to our MOLA cross sections, the final horizontal location accuracy is at the level of 1–3 MDIM pixels (i.e., within 200–600 m or ~1–2 MOLA footprints). All MOLA topographic profiles presented in this paper have been carefully registered to the MDIM images as part of our assessment process. This is critical when parameters related to volumes are estimated since off-center topographic profiles can provide extremely misleading values for all properties computed via numerical integration (Garvin and Frawley 1998). Of the ~100 craterforms sampled by MOLA (Fig. 1), over 30% were traversed within 20% of their central axes of symmetry. Cratered cones sampled by MOLA were considered in this study only if the topographic cross section bisected the axis of symmetry.

GEOMETRIC PROPERTIES

MOLA traversed the cavities of 109 impact features north of about 57°N. More than 30% of these traverses provided near

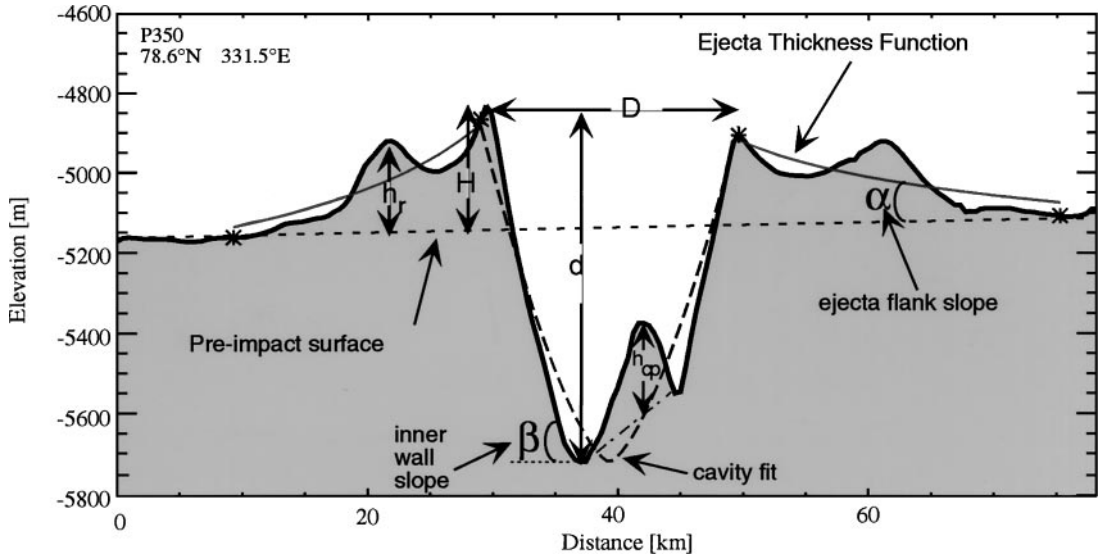

FIG. 2. Example of a polar impact crater cross-section acquired by MOLA indicating some of the measured parameters considered (see Table I). The crater shown is that illustrated in Fig. 6.

centerline cross sections which permit first-order assessment of depth–diameter relationships, as well as correlation of cavity volumes and shapes with crater diameter. While MOLA will eventually sample thousands of fresh martian craters in all major surficial geologic units, the recent SPO data provide an interesting preliminary examination of the polar region craters in contrast with craters from other latitudes and terrain types. We have adopted 57°N as the edge of the polar terrains on the basis of the existence of winter frost on the surface (Thomas *et al.* 1992) north of this latitude. This allows us to include most of the north polar region geologic units in one group. We endeavored to consider topographically "fresh" impact craters, but recognize that assessment of degradation state from MOLA profiles and analysis of MDIM images is imperfect. Barlow and Bradley (1990) and Strom *et al.* (1992) describe the fresh crater population on Mars at most latitudes between $+60°$N and $-60°$S on the basis of extensive morphologic analyses. In this study, we use the sharpness of rim topography and other cavity characteristics, including floor geometry, to identify minimally degraded craters in the region north of 57°N. When developing scaling laws that relate depth, volume, and cavity shape to crater diameter (D), we considered only the subpopulation of minimally degraded craters. To further remove outliers, we restricted all of our least-squares regression analyses to those samples less than one standard deviation in depth from the sample mean.

For specific geometric properties, one interesting assessment of the geometric properties measured from MOLA profiles (Fig. 2; Table I), is to compare the entire population of North Polar Region impact craters with those for nonpolar latitudes, as was accomplished for the Moon (Pike 1980b) and for examples on Earth (Roddy 1977). We have taken this approach to assess crater cavity shapes, ejecta thickness functions (ETF), and cavity volume properties. In particular, for the subset of north polar region craters associated with ice or frost we have measured the above morphologic characteristics from MOLA topographic profiles and compared them to the entire population of north polar region (nonpolar) impact craters.

For example, we have measured the cross-sectional shape of the crater cavities using a function of the form: $z = kx^n$, where z is the surface elevation relative to the floor, x is horizontal distance from the crater center, and k and n are least-squares regression fit parameters. Previously, we observed that the n-parameter is a reasonable indicator of cavity shape for nonpolar craters (Garvin and Frawley 1998), with n values between 2 and 3 for most complex northern hemisphere craters, and we would expect it to also be a reasonable cavity shape indicator for polar craters as well.

We estimate an ejecta thickness function using an approach first developed by McGetchin *et al.* (1973) and recently applied to martian impact craters by Garvin and Frawley (1998). This function describes the decay of ejecta topography from the rim crest to the edge of the continuous ejecta blanket using a simple function of the form $t_e = k(r/R)^b$, where t_e is the ejecta thickness as a function of radial distance r from the rim crest, R is the rim crest radius, and k and b are least-squares regression constants. Melosh (1989) and McGetchin *et al.* (1973) suggested on the basis of explosion experiment data that the exponent b should typically fall in the -2.5 to -3.5 range, depending on several factors, including kinetic energy of impact. Recently, Garvin and Frawley (1998) showed that while there is a general tendency for overall b values of martian craters to fall in this range, the most common b values for Northern Hemisphere (nonpolar) craters was -0.5 ± 0.3. This is substantially different than the Melosh (1989) and McGetchin *et al.* values (1973). It is interesting to compare the ice-associated martian craters to the overall martian

crater values, since one possible explanation of the difference is that the analyses of martian ejecta thickness do not take into consideration the structural uplift of the rim crest, which is difficult to model at this time for martian impact craters.

DEPTH VERSUS DIAMETER CORRELATIONS

The distinction between ice-associated polar region impact craters and those from the remainder of the northern hemisphere is most striking when crater depth from the rim crest (d) is related to rim crest diameter (D). The polar region craters follow a power law of the form $d = 0.03\,D^{1.04}$, where d and D are measured in kilometers. This relation has been computed on the basis of our sample of complex impact craters larger than 6 km, which is the best fit (± 0.5 km) for the simple-to-complex crater transition diameter in the North Polar Region as determined from MOLA-derived geometric properties (Garvin and Frawley 1998) and which is in general agreement with that suggested by Pike (1988). In contrast, the nonpolar unit complex craters are best fit by a power law of the form $d = 0.19\,D^{0.55}$, where d and D are again measured in kilometers. This relationship includes impact craters in the nonpolar regions of Mars observed during the early MGS mapping mission (Garvin *et al.* 1999). The difference between a power-law with an exponent of 1.04 (polar) and 0.55 (nonpolar) is statistically significant and has substantial consequences; for diameters larger than 43.2 km, polar complex craters will be deeper than nonpolar counterparts of a similar diameter. Ice-associated craters north of 70°N appear to follow an even steeper power law, as they display apparent cavity floor depths in excess of the general polar region trend.

Indeed, as we shall discuss in an upcoming section, we have observed that a majority of martian craters associated with ice or frost are deeper than simple models of the d versus D overall or northern hemisphere relationships would suggest. We use an additional comparison of observed depth with estimated depth of excavation to consider d versus D variations from region to region. Previously, Barlow and Bradley (1990) used an approach suggested by Croft (1985) to estimate the depths of excavation (d_e) of martian impact craters with an equation of the form $d_e = k\,D_a^{0.85}$, where k is a constant related to the simple-to-complex transition diameter and D_a is the final, apparent cavity diameter at the rim crest. Using the MOLA-based value of 6 km for the transition diameter, we derive a simple equation of the form

$$d_e = 0.131 D_a^{0.85},$$

from which we can estimate the maximum depths of excavation. This relationship indicates the theoretical depth of excavation in the north polar region of Mars is usually much greater than the observed apparent crater depths as measured by MOLA. For a 20-km-diameter crater, the difference ($d_e - d_a$) is ~1 km, while for a 40-km feature, it is over 1.6 km. It rises to nearly 2.5 km at a diameter of 80 km. Thus, relative to a modeled depth of excavation, there is considerable slumping and modification stage fallback into complex crater cavities on Mars before erosional modification. For complex craters larger than 11 km in diameter, the depth of excavation is predicted to be at least 1.0 km, while for *Korolev*-scale features (80 km diameter), it could be as large as 5 km. For most of the polar impact craters sampled by MOLA, the difference between the model depth of excavation and the apparent depth of the cavity is hundreds of meters to kilometers, but there are a few cases where the apparent depth (d_a) exceeds that predicted as the depth of excavation. We will return to this issue when we consider specific examples.

CAVITY VOLUME AND SHAPE

If one considers how cavity volume (V) relates to crater diameter (D), polar versus nonpolar crater differences again emerge. We find that for polar region impact craters, $V = 0.01\,D^{3.03}$, where V (km^3) is measured by numerical integration of near-centerline MOLA cross sections. D is in kilometers. For nonpolar region craters, the relationship is $V = 0.04\,D^{2.68}$, suggesting that polar crater cavities are volumetrically larger than those in other regions. Indeed, for crater diameters larger than ~52 km, cavity volume is always greater for polar impact features than for craters at lower latitudes. The larger volume for polar craters may be a consequence of target properties that enable enhanced excavation at high kinetic energies. When examining the V versus D relationship for polar craters in comparison with that for nonpolar ones, we consistently observe a break in slope at approximately 6 km, suggesting that the simple-to-complex transition may be close to 6 km, as previously suggested (Pike 1988).

For cross-sectional cavity shape, the exponent (n) that describes the order of the best-fitting polynomial can be correlated with crater diameter. We then may consider the relationship between cavity shape, crater diameter, and crater location. For polar craters, cavity shape exhibits a power law of the form $n = 2.22\,D^{-0.05}$, while for nonpolar craters, the relationship is $n = 2.28\,D^{0.01}$, where D is in kilometers. Together, these power laws suggest that there is a strong tendency for craters to become more paraboloidal with increasing diameter, independent of location.

It is also interesting to compare the measured cavity volume with estimated volume of excavation from models. Where MOLA cross-sections have sampled the central region of a crater cavity (i.e., within 20% of the crater's central axis of symmetry), we employ numerical integration methods to estimate the cavity volume (V) (Garvin and Frawley 1998) as it compares to the modeled volume of excavation (Melosh 1989, Grieve and Garvin 1984, Croft 1985). Excavation volumes can be estimated using an equation of the form

$$V_e = (\pi/48)\,D_t^3,$$

where D_t is the diameter of the excavation cavity, which can be taken as being equivalent to the diameter of the transient

cavity. If we adopt Croft's (1985) approximation such that $D_t = (D_h^{0.15})(D_a^{0.85})$, where D_h is the simple-to-complex transition (i.e., approximately 6 km on Mars on the basis of this study), then we can estimate the expected volume of excavation for martian craters (V_e) using

$$V_e = 0.147\, D_a^{2.55},$$

where D_a is the apparent rim-crest diameter in kilometers. This model volume of excavation (V_e) carries with it an underlying assumption that a Z model with $Z = 3$ is appropriate for martian fresh impact craters in the 6- to 80-km-diameter range (Croft 1985, Grieve and Garvin 1984). For representative martian north polar region impact craters, the predicted V_e from the above equation is typically two to three times the apparent volume measured by MOLA. We will return to the significance of this fundamental disparity after examining several specific martian impact features.

RIM HEIGHTS

The rim heights for fresh and minimally degraded impact craters, relative to the preimpact surrounding surface, has traditionally been difficult to measure with high reliability for Mars (Pike 1980b). MOLA topographic profiles permit improved assessment of relative rim relief. The mean rim heights (H) for polar region craters (0.253 km) is not statistically different from that for nonpolar craters (0.219 km). However, this simple statistical analysis does not take into account levels of rim flank burial, which is likely to be large in higher latitude settings on the basis of high-resolution Viking images. The mean depth (as measured from the rim crest to the lowest point on the floor) is 0.57 km for polar region craters and 0.63 km for nonpolar region examples. We note that the depth–diameter scaling laws demonstrate a major difference in polar region crater depths relative to nonpolar varieties. However, such differences in polar versus nonpolar rim height are within 1/10th of a standard deviation of the mean and are not considered meaningful.

EJECTA THICKNESS FUNCTION

When we consider the topographic character of the continuous ejecta blankets using the ETF function $t_e = k(r/R)^b$, described previously, there are appreciable differences between polar and nonpolar impact features for the mean ETF exponent (b). For polar region craters, the mean $b = -3.73$, with a modal value of -0.50; for nonpolar craters $b = -2.30$, with a modal value of -0.10. In both cases, the dynamic range of b values extends from -0.1 to -8.0. None of these mean or modal values lies within the previously described acceptable range (-2.5 to -3.5) as suggested by Melosh (1989). However, the variability in the characteristics of the ETF for Mars are large, and the standard deviation on the mean values cited above is in excess of 3.0. We suggest that ejecta topology is related to latitude and hence to aspects of target type, but as yet we have insufficient statistics to unravel the subtleties.

EJECTA VOLUME VERSUS CAVITY VOLUME

One final geometric indication that north polar region impact craters on Mars behave differently from their nonpolar counterparts is apparent in the ratio of ejecta volume to cavity volume (V_{ej}/V), where V_{ej} is the apparent ejecta volume of the continuous ejecta blanket (CEB) as defined by means of MOLA topography and Viking images, and V is the cavity volume as defined above. For near-centerline MOLA cross-sections, we can estimate V_{ej} and normalize it to the apparent volume of the crater cavity to compute the V_{ej}/V ratio. Garvin and Frawley (1998) treated this parameter for several dozen impact features in the martian mid-latitudes, and here we extend earlier work to include over 100 craters in the Northern Hemisphere. We find the mean V_{ej}/V ratio for polar region craters to be 2.3, while that for nonpolar craters is 1.14. In both cases the dispersion about the mean value is large. However, once again we observe that minimally degraded impact features in the high northern latitudes are fundamentally distinctive from their mid-latitude counterparts. The most probable explanation for this disparity is the variability of cavity fill in the polar region. While there is evidence of ejecta modification and possibly burial in the polar region, there remains a readily observed topographic expression of most continuous ejecta blankets on the basis of MOLA data. However, it is more difficult to assess the level of cavity infill from single topographic cross sections or Viking images alone. In combination, however, we believe we have evidence of significant levels of cavity infill in the highest northern latitudes of Mars, as quantified by MOLA topographic data. We will treat this evidence using specific examples in the sections that follow.

ICE-ASSOCIATED CRATERS

During the MGS Science Phase Orbit period MOLA sampled 14 impact features and one probable volcanic feature for which there is an association with high-albedo frost or ice deposits apparent from Viking Orbiter images (MDIM's at 234 m/pixel or higher resolution Viking images in the 40 to 100 m/pixel resolution range). Table II summarizes some of the salient geometric properties of those ice-associated craters along with one volcanic feature where the MOLA coverage permits reliable computation of volumes. Table III summarizes modeled parameters for the ice-associated features discussed in the examples below. For most of the impact craters sampled by MOLA north of 72°N, the topographic characteristics of the crater cavity are unlike those typical of other craters on Mars (Garvin and Frawley 1998). Here we treat several end-member cases in order to address issues associated with north polar region modification processes and rates.

TABLE II
Geometric Parameters for Ice-Associated Impact Craters Observed by MOLA on Mars

Feature	Location	Diam (km)	depth (km)	H_{rim} (km)	d/D	Cavity slope	V_{cav} (km^3)	Cavity shape	d_{mod} (km)	Infill (km)	V_{mod} (km^3)	V_{infill} (km^3)
A	81°N, 190°E	19	0.92	0.28	0.048	15	124	4.7	0.64	—	183	59
B	77°N, 89°E	34	0.66	0.71	0.020	14.5	311	2.2	1.17	−0.51	559	248
C	79°N, 331°E	20	0.85	0.28	0.043	7.9	122	2.8	0.68	—	156	34
D	77°N, 215°E	44	2.1	0.98	0.049	15.8	1075	4.1	1.54	—	1538	463
E	73°N, 163°E	84	2.2	0.91	0.027	11.2	5800	1.8	2.86[a]	−0.62	7840[a]	1356[a]
F	81°N, 255°E	18	0.59	0.11	0.033	5.0	103	1.6	0.61	−0.02	68	35
G	77°N, 195°E	20	0.92	0.35	0.046	12.6	126	1.9	0.66	—	128	2.5
H	79°N, 62°E	18	0.81	0.32	0.046	11.3	97	1.9	0.60	—	100	3.4
I	72°N, 345°E	20	1.47	0.45	0.074	15.6	215	1.8	0.68	—	219	4
J	73°N, 38°E	9	1.02	0.32	0.113	20	31	1.8	0.29	—	31	—
	75°N, 341°E	16	0.38	0.13	0.024	10.0	40	2.3	0.54	−0.16	58	18
	76°N, 159°E	14	0.51	0.19	0.036	10.1	42	2.2	0.47	—	41	—
	77°N, 46°E	11	0.30	0.22	0.026	8.9	18	3.0	0.36	−0.06	21	—
	74°N, 319°E	13	0.54	0.25	0.041	12	32	1.6	0.43	—	32	—
	85°N, 2°E	11	1.08	0.10	0.10	16	39	1.2	0.36	—	31	—

Note. d_{mod} is cavity depth modeled using the general North Polar Region depth-diameter power law. Infill is $d_{mod} - d_a$, where d_a is observed (by MOLA) cavity depth. Nonphysical values are indicated by "—" and are due to enhanced apparent cavity depths relative to the entire population of polar region impact features. Negative values indicate the depth of infill in km. V_{mod} is a model cavity volume computed using the apparent cavity shape (measured by MOLA) and an equation given in the text that relates shape, diameter D, and depth d_a to volume. This is not equivalent to an excavation volume. See text for definition of cavity shape. V_{infill} is the $V_{mod} - V_{cav}$, where V_{cav} is the observed cavity volume as measured by MOLA. This is a proxy for a cavity interior infill volume. Nonphysical values are indicated by "—" and suggest that the cavity is not infilled beyond the level that would be predicted by the typical cavity shape, diameter, and depth. The crater located at 85°N, 2°E (last row in table) is a suspected impact crater for which inadequate Viking era images are available to assess its morphology. We have included it because it could represent a fresh impact feature in the margin of the ice cap.

[a] Values are derived from a DEM rather than the centerline pass in Fig. 8. See text for discussion.

FEATURE "A": ICE-ASSOCIATED COMPLEX CRATER IN POLAR DUNES (82°N, 190°E)

Figure 3 illustrates a 19-km-diameter impact crater located within the Olympia Planitia dune fields (designated A in Fig. 1). This feature clearly cuts the transverse dune deposits and has an apparent depth of 0.92 km. Its aspect ratio (d/D) is 0.048, a value larger than is typical of craters in this size range (0.034) elsewhere on Mars. The depth more statistically typical of a crater of this size is 0.64 km, indicating that this crater is 280 m

TABLE III
Modeled Parameters for Ice-Associated Craters Discussed in the Text

Feature	Crater location	Diameter (km)	Apparent depth, d_a (km)	Model depth, d_m (km)	Infill thickness (km)	Vol. infill thickness (m)	Ejecta thickness (m)	MOLA floor elevation (m)
A	82°N, 190°E	19	0.92	1.06	0.140	295	43	−5000
B	77°N, 89°E	34	0.66	1.41	0.750	708	52	−4450
C	79°N, 331°E	20	0.85	1.09	0.235	189	54	−5750
D	77°N, 215°E	44	2.1	1.60	—	514	124	−6000
E	73°N, 163°E	84	2.2	2.19	—	557	123	−6250
F	81°N, 255°E	18	0.59	0.81	0.220	—	48	−4700
G	77°N, 195°E	20	0.92	1.09	0.165	18	70	−5450
H	79°N, 62°E	18	0.81	1.03	0.220	31	72	−4950
I	72°N, 345°E	20	1.47	1.09	—	32	47	−6100
J	73°N, 38°E	9	1.03	0.734	—	—	33	−6000

Note. Model depth d_m is that computed from $d = 0.25\,D^{0.49}$ fit for complex N. Hemisphere craters (Garvin and Frawley 1998). This is not the same as d_{mod} from Table II. Infill thickness is $d_m - d_a$, where d_a is apparent depth from rim crest. Vol. infill thickness is model cavity volume minus apparent cavity volume, divided by the apparent surface area of the crater floor (see Table II and text). Ejecta thickness is average thickness of entire continuous ejecta blanket as computed from the apparent volume of ejecta divided by the surface area of the ejecta (from MOLA). MOLA floor elevation is the absolute minimum floor elevation as measured by MOLA in meters relative to the MOLA defined equatorial radius of Mars (Smith *et al.* 1998). "—" is indicated when the computation results in a nonphysical value (i.e., when the apparent depth is greater than the model depth).

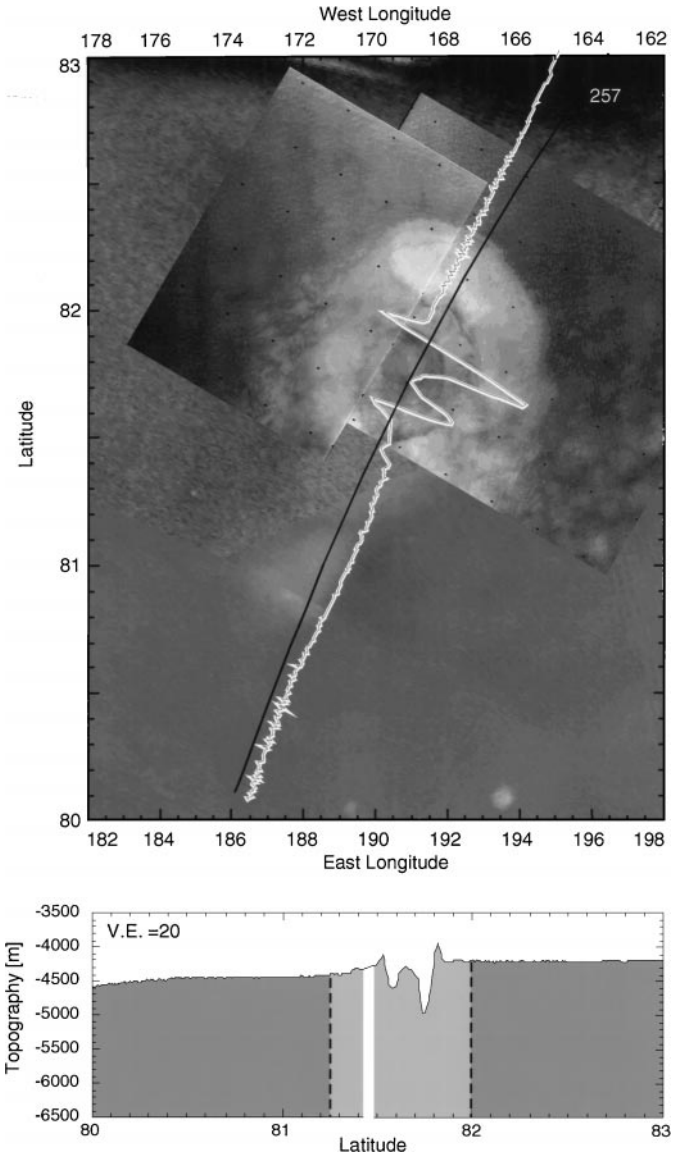

FIG. 3. Example of a 19-km-diameter crater located at 82°N, 190°E within the *Olympia Planitia* dune fields. (Top) The best available Viking Orbiter image, with MOLA profiles superimposed. (Bottom), The MOLA cross section, with the observed limits of ejecta indicated (dashed lines). The white region indicates where MOLA encountered clouds and was unable to make surface observations. All upcoming crater figures use this general format (i.e., Viking image with MOLA profile below). Note that this is crater A in Fig. 1.

deeper than would be predicted using the depth–diameter scaling law described above. The crater cavity displays an n value of 4.7, which suggests that the preerosion interior was very "U" shaped for a crater of this size. The ejecta thickness function exponent (b) varies enormously from a very typical value of -0.9 in the northern ejecta to -11.8 on the southern rim flank. However, as can be observed in Fig. 3, the boundaries of the continuous ejecta deposit are very poorly constrained by either MOLA or Viking image data. The subtleties of the MOLA topographic profile indicate that dune deposits may have overridden ejecta-related topography associated with this crater. This is also suggested by the MDIM image (Fig. 3). Furthermore, on the basis of dune properties measured by MOLA (Zuber *et al.* 1998), the average height of dunes in this region is 25 m, which is enough to blanket 20-m-tall ramparts.

The unique topology of the cavity infill deposits at this crater, relative to what can be observed in a high-resolution Viking image (Fig. 3), first drew our attention to it. The cross-sectional shape of the cavity interior deposits is not typical of nonpolar region impact craters. The "shape" of the cavity infill deposit is similar to volcanic lava domes on Earth (Garvin 1996) and is atypical of the sample of central peaks observed by MOLA to date. The elevation of the peak of the cavity interior deposits is similar to that of the surrounding preimpact surface. This has not been observed elsewhere on Mars for any of the central peak or central peak-pit craters sampled by MOLA (Garvin and Frawley 1998). The ratio of the volume of the central deposit (V_{cd}) to that of the apparent cavity (V) plus all interior deposits (i.e., $V_{cd}/[V + V_{cd}]$) is 0.35, indicating that more than 35% of the apparent cavity is filled with materials.

We can model the preerosional cavity for craters such as this by estimating their diameter-dependent depths and cavity shapes using the empirical scaling laws discussed previously. Once we have modeled the depth and cavity cross-sectional shape, we can use a simple equation of the form

$$V_m = [\pi n D^2 d]/[8 + 4n],$$

where D is diameter in kilometers, d is model depth in kilometers, n is model cavity cross-section, and V_m is the reconstructed or modeled cavity volume in km^3. Using this approach, we estimate a preerosional cavity volume V_m of 183 km^3. The difference between the apparent cavity volume measured by MOLA (V) and the modeled volume (V_m) is the estimated total volume of cavity infill (V_{inf}). For this crater, we find that V_{inf} is $\sim$59 km^3, which is 48% by volume of the original cavity. We have followed this approach for all of the craters listed in Table II. If we compute the volume of excavation for this crater within the Olympia Planitia region, we find that V_e is 267 km^3 or $\sim$2 times larger than the apparent volume (124 km^3). The difference between V_e and the apparent cavity volume V is 143 km^3, which is 2.4 times larger. We attribute this discrepancy in part to the approximations intrinsic to a volume of excavation computation, as well as to modification stage slumping which will serve to reduce the final cavity volume by up to 50% (Melosh 1989). The estimated volume of cavity infill (59 km^3) and a corrected modification-stage cavity volume are in agreement at 10–20% levels. Thus, we believe that this 19-km crater (Fig. 3; see also Table II) provides evidence of significant cavity infilling due to postcrater formation processes.

The area of the apparent cavity floor is $\sim$150 km^2. We can estimate the thickness of the cavity infill deposit by assuming that the infill volume estimation is reasonable and computing the ratio V_{inf}/SA, where SA is the true surface area of the cavity

floor. A uniform layer ∼300 m thick is the result. We observe, however, a plug-like (i.e., with "snow-cone" appearance) central cavity deposit geometry here and in other ice-associated craters on Mars. Most cavity infill deposits are not manifested as uniform thickness layers in the floors of these high-latitude impact features. Finally, the MOLA-based estimate of the volume of the central deposit (V_{cd}) suggests that it is ∼69 km^3, which is similar to within 15% of the independent estimate of cavity infill (59 km^3).

There is some indication that the Olympia Planitia dunes may form a carapace of sediment that overlies stagnant polar cap "ice" (Zuber *et al.* 1998). If this is the case, the 19-km crater depicted in Fig. 3 must have excavated through the 20–40 m of dune sediments to encounter buried ground ice. An excavation flow field established in a layered target consisting of dune sediments atop ground ice of unknown thickness has not been completely treated previously (Clifford 1993, Melosh 1989). If we take the model depth of excavation (1.6 km), together with a simple Z-model approach as discussed above, we can consider the volumes of materials involved. The anomalous cavity shape, central cavity deposit shape, and large volume of infilling materials relative to the total cavity volume (59 km^3 versus 124 km^3), suggest that this impact feature developed differently than similar 20-km-diameter craters in nonpolar target materials. More typical 20-km-diameter impact features within polar units (i.e., the crater at 72°N, 345°E, shown as Feature I in the Fig. 1 location map and discussed later) display negligible cavity infill volumes.

The ejecta flank slopes for the crater in Fig. 3 (∼0.9°) are similar to those measured for impact craters elsewhere on Mars (Garvin and Frawley 1998). This observation supports the argument that it is not heavily eroded. If this feature is relatively unmodified, then one possibility is that the enhanced cavity deposit volume is due to melting of ground ice within the cavity (Squyres *et al.* 1992). Alternately, this crater could have been totally buried by a recent advance of the north polar cap, essentially filling its cavity as a consequence. Subsequent cap retreat and ice ablation could have left behind large volumes of cavity infill, more difficult to erode by wind or solar illumination than those in the surrounding plains. Current estimates (Thomas *et al.* 1992) for polar sedimentation rates allow for the deposition of an equivalent thickness of ∼300 m of infill in less than 43 million years. The higher sedimentation rates associated with layered bands in the north polar region, could allow for development of a layer 300 m thick in ∼10 million years. However, if we take the average relief of central deposit (0.54 km) as the typical infill thickness, it would require 20 to 80 million years of continuous deposition to accumulate. We can conclude only that episodic high sedimentation rate or ice-accumulation processes have filled this impact feature in such a way that the erosion of the infilling materials has not restored the original cavity interior geometry.

An alternate working hypothesis for this and other ice-filled impact craters sampled by MOLA involves mobilization of a weak, ice-rich layer. If the crater formation process were to enable late-stage inner cavity floor melting, then an artificially elevated cavity floor could develop, only to decay at its margins in the initial stages of subsurface withdrawal, cooling, and surface ablation. If this process were at work on the crater in Fig. 3, it would suggest that a considerable volume of ice were available near the depth of excavation level (1.6 km) in the martian crust. This is consistent with the hypothesis that the Olympia Planitia dunes overlie a buried portion of the polar ice cap (Zuber *et al.* 1998). Improved geometric constraints on the topology of the cavity floor and infilling deposits are needed to further test this alternate hypothesis.

FEATURE "B": EXTENSIVELY INFILLED CRATER AT 77°N, 89°E

An example of an ice-associated crater with extreme levels of cavity infill is illustrated in Fig. 4 (crater B in Fig. 1). In this case a 34-km crater was sampled by two discrete MOLA cross sections in July of 1998. This ice-associated crater is located at 77°N, 89°E and has a total depth of 0.66 km, and a d/D of 0.020 (see Table II). Its rim height variability (over 300 m relative to the preimpact topography of the region) is the highest found so far for martian craters of this size. Furthermore, the level of cavity infill rises above the surrounding preimpact surface, similar to what has been observed by MOLA for certain pedestal craters on Mars (Garvin and Frawley 1998). A nearly perfect center-line pass, acquired on MGS orbit 415, illustrates the geometry of the perched infilling deposits. The overall cavity interior shape, on the basis of both MOLA transects, indicates an n-value of 2.2 (paraboloidal), which is consistent with nonpolar craters of this diameter on Mars (Garvin and Frawley 1998). Possibly dune-mantled ejecta ramparts with more than 50 m of relative relief are also observed 10 to 20 km from the rim crest.

If one reconstructs the preerosion cavity geometry for this feature (Fig. 5), it is clear that ∼80% of the apparent cavity is filled with interior deposits whose asymmetric spatial distribution indicates that they are not controlled by underlying central uplift topography. In comparison, the irregular geometry of the cavity interior deposits associated with the impact feature discussed previously (Fig. 3) constitute ∼50% of the reconstructed cavity (Fig. 5b). Typical average ejecta flank slopes for the crater illustrated in Fig. 4 are ∼1.2°, with local peak values as high as 12° near the rim crest. Cavity wall slopes average ∼14.5°, similar in magnitude to those measured for the crater illustrated in Fig. 3. The topographic expression of the crater rim and inner cavity wall and the topographically well-defined continuous ejecta blanket suggest that this feature is not highly modified in spite of what a first glance at the high-resolution Viking Orbiter image would lead one to believe (Fig. 4c).

The preerosion cavity volume expected for a 34-km impact crater with a cross-sectional shape (n) of 2.2 and a reconstructed total depth of 1.2 km (i.e., from the $d - D$ power law discussed previously) is ∼560 km^3 (Table II). The measured apparent volume of the crater cavity plus that of the topographically

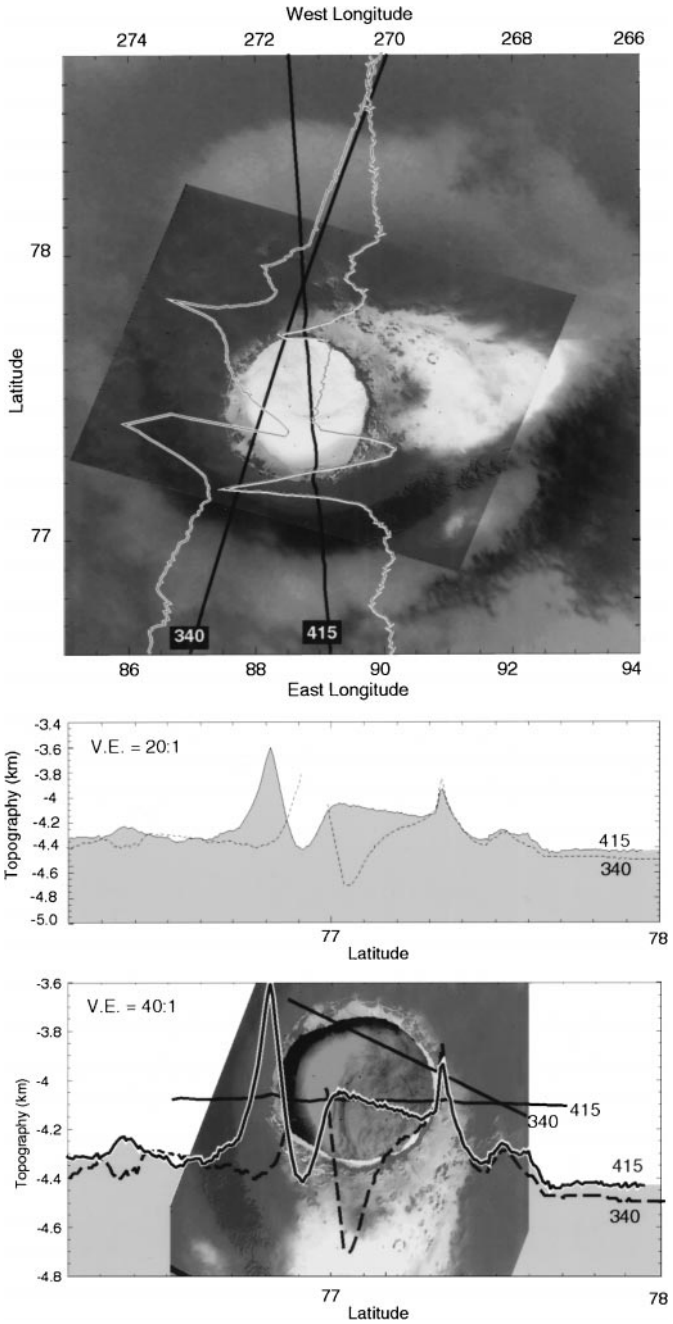

FIG. 4. Example of an extensively infilled 34-km-diameter crater located at 77°N, 89°E (Feature B in Fig. 1). (Bottom) The topology of the crater floor in higher detail, revealing tilted escarpments ~10 m in height along the centerline pass (MGS orbit 415).

defined central deposit is ~378 km^3. Allowing for the rim height asymmetry of ~300 m, this indicates that ~80% of the original (preerosion) cavity has been infilled. If we examine MGS orbit 340 (Fig. 4b) and its slightly off-center coverage of this crater, it appears that the cavity depth is at least 60 m greater than that measured from the centerline profile. Thus, we estimate an average depth of infill to be on the order of 500 m. To accumulate this thickness using presently accepted sedimentation rates for the north polar region (Howard *et al.* 1982, Thomas *et al.* 1992) could require between ~17 to 71 million years, assuming constant, continuous deposition.

Of particular interest are the shorter-wavelength features on the upper surface of the cavity interior deposits. In Fig. 4 (c), these features are displayed at full resolution. A staircase-like pattern of possible benches or escarpments, tilted less than 1° toward the north, can be observed. The average MOLA-based relief of these benches is 10 ± 3 m, and each bench is typically 1–2 km across. These staircase features are reminiscent of certain types of banded layers in the polar layered terrain. The high-resolution Viking Orbiter image displayed in Fig. 4c indicates that these escarpments are curvilinear, and that they could mark areas of relatively rapid localized erosion, perhaps caused by rapid defrosting, ablation, or other processes (Thomas *et al.* 1992). The appearance of these staircase-like features within a moderately degraded impact feature could provide a constraint on layer thickness properties throughout the North Polar Region. Perhaps the layers exposed in the crater are similar to the 10- to 50-m-thick bands that are widespread and well-documented in the northern polar layered deposits (Howard *et al.* 1982, Thomas *et al.* 1992). MOLA observations of the cross-sectional properties of polar dunes (Garvin and Frawley 1999) suggests that the staircase-like features are not representative of any of the duneforms that are adequately resolved by the sampling characteristics of the laser altimeter (i.e., approximately 330 m along track).

Grieve and Cintala (1992) have developed a model for impact melt generation that Clifford (1993) applied to Mars. For a given crater of apparent diameter D, the impact melt model permits consideration of the volume of melt assuming vertical impacts of a chondritic projectile into the martian surface at 10 km/s. For a 34-km-diameter impact crater on Mars (i.e., Fig. 4), the Grieve and Cintala (1992) model would suggest that ~67 km^3 of melt could be produced. This impact melt could remain in the cavity or mobilize ground ice as described by Clifford (1993). If this melt volume were uniformly distributed over the cavity floor area of ~700 km^2, it would result in a layer thickness of ~95 m, which is inadequate to explain the 500-m thickness of apparent infill. A reduction in the volume of cavity infill (248 km^3), due to postimpact sedimentary or ice-related processes, of ~90 km^3 would lessen the fraction of cavity infill to ~50%, which is consistent with that computed for the crater in Olympia Planitia (Fig. 3).

FEATURE "C": ICE-ASSOCIATED COMPLEX CRATER AT 79°N, 331°E

A particularly well-sampled impact feature 20 km in diameter was bisected on two occasions by MOLA cross sections (Fig. 6). This complex impact structure is located within 50–60 km of the perennial north polar cap (crater C in Fig. 1). In addition, it is at least 850 m deep, with a 280-m rim, relative to the preimpact surrounding surfaces. Dune deposits appear to mantle ice

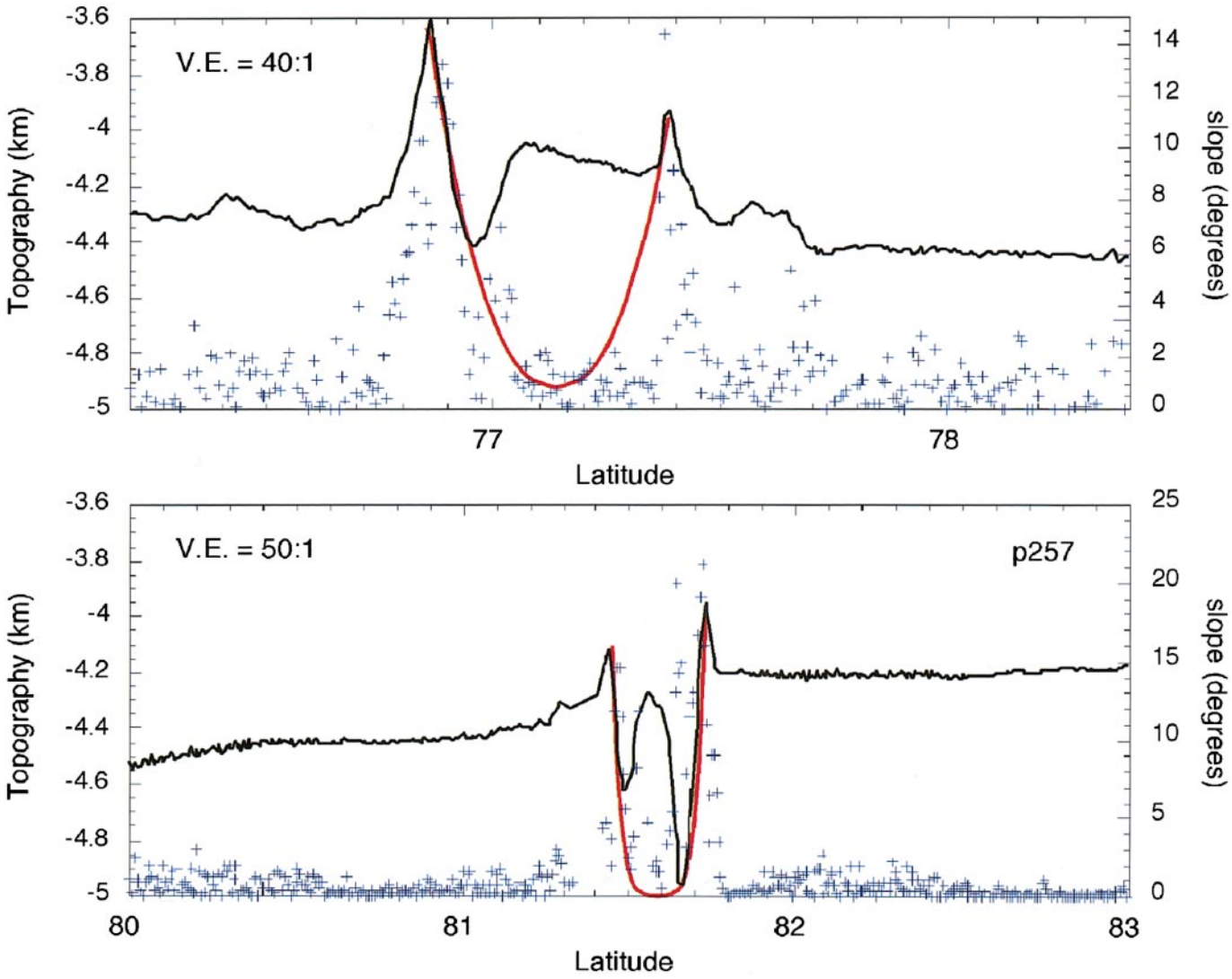

FIG. 5. Cavity reconstructions for ice-associated craters illustrated in Figs. 3 and 4. (Top) The MOLA cross section for the crater shown in Fig. 4, with a model cavity reconstruction superimposed. (Bottom) The MOLA cross-section for the crater illustrated in Fig. 3, with a model cavity reconstruction. Sub-kilometer-scale local slopes computed from MOLA profile data are superimposed as "+" symbols in each case. Cavity wall slopes as high as 15° to 20° were observed.

deposits within the cavity interior (Fig. 6). Unlike the previous examples (Figs. 3 and 4), the typical inner cavity wall slopes for this feature are 8°, compared to the 14°. In many respects, the geometric properties of this feature (Table II) are similar to those observed for the crater illustrated in Fig. 3. The cavity cross-sectional geometry or shape is somewhat more U-shaped than is typical of 20-km impact features, and the ratio of ejecta to interior cavity volume (V_{ej}/V) is 3.2, significantly greater than that observed for most polar region impact features. For a feature of this size, the Grieve and Cintala (1992) impact melt volume would be ∼12 km^3, which is less than 10% the apparent volume of the cavity. Using the depth–diameter scaling relationship introduced previously, the model depth for this feature is 0.68 km, while the apparent depth, as measured by MOLA on two independent passes is greater than 0.85 km. As with the feature at 81.6°N, 189.9°E (Fig. 3), the implication is that this crater is deeper than one would anticipate (Table III). Indeed, if we consider the general northern hemisphere depth–diameter relationship suggested in Garvin and Frawley (1998), the expected depth would be 1.07 km, suggesting a level of cavity infill of 0.230 km. As discussed previously, the general North Polar Region impact craters are shallower at small diameters than their mid- and equatorial-latitude counterparts, but above about 40 km, they are statistically deeper. For 20-km craters such as those shown in Figs. 3 and 4, the apparent depths are more similar to nonpolar impact features than to their polar counterparts.

As with the previous examples, we can model the cavity volume for feature "C" (Fig. 6) using the scaled depth and cavity shapes. The model preerosion volume is 34 km^3 in excess of that observed (see Table II), indicating that at least 28% of the cavity

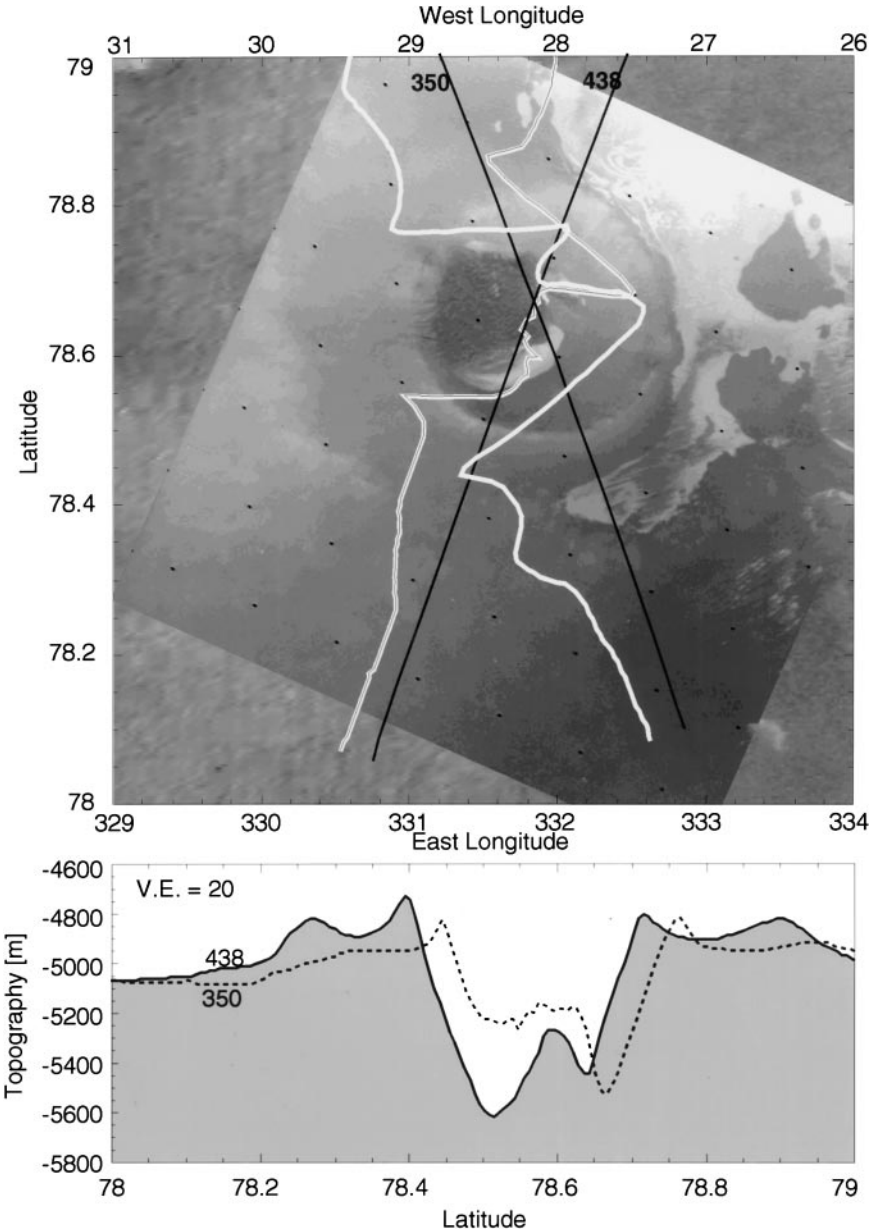

FIG. 6. Example of a well-sampled 20-km-diameter crater located at 79°N, 331°E (Feature C in Fig. 1). Two crossing MOLA centerline profiles traversed this crater, which appears to be filled with dune-covered ice deposits.

is infilled with polar sediments and ice. The computed volume of excavation for this crater is 305 km^3, or 183 km^3 larger than the apparent cavity volume measured by MOLA. If we allow for modification stage slumping, the overall apparent volume of the observed cavity (i.e., the cavity volume V plus the volume of the central deposit V_{cd}) is 183 km^3, which is within 30 km^3 of the expected volume of the preerosion cavity. The 34 km^3 of apparent infilling materials, when spread as a layer of uniform thickness across the ~200 km^2 area of the cavity floor, would contribute a thickness of at least 170 m. This is exactly the amount of excess depth (relative to the general depth–diameter relation for the polar region) observed. Therefore, we conclude that on the order of 30% of the original cavity is filled with postformation ice and sediments. The shelf-like geometry of the central deposits at this crater (Fig. 6) is similar to that of other ice-associated craters. Its estimated volume, relative to the deepest point of the cavity floor, is no more than 61 km^3 and more plausibly on the order of 40 km^3. This is within 20% of the independently computed volume of infill (Table II).

Our conclusion is that the crater depicted in Fig. 6 is moderately infilled by materials that contribute to the lowering of its modeled cavity volume. Accumulation of at least 34 km^3 of

materials in a closed depression such as an impact crater may have required 6–27 million years (Thomas *et al.* 1992, Howard *et al.* 1982) and possibly longer if the most conservative polar sedimentation rates are invoked (<7 m per million years). Removal of 0.85 to 0.92 km of covering materials is another matter, as rates of removal via stripping or ablation are poorly constrained (Howard *et al.* 1982, Plaut *et al.* 1988, Craddock *et al.* 1997). It is unclear whether this 20 km diameter crater experienced wholesale burial and subsequent exhumation, as was discussed previously for the 34-km crater shown in Fig. 4. The minimum crater floor depth for this feature is ∼240 m, as measured relative to the surrounding preimpact surface. This does not indicate whether or not the cavity interior deposits ever reached above the preimpact surface, as is observed at the craters in considered previously (Figs. 3 and 4).

The topology of the ejecta within 1–2 radii of the rim crest for this crater (Fig. 6) is potentially significant. Unlike many ice-associated craters, the near-rim topography of the continuous ejecta blanket displays a relative relief or thickness that is within a few tens of meters of the rim crest. The rim crest is sufficiently sharp in Viking images and in topographic character from MOLA measurements to disfavor a severe rim erosion scenario. An alternate explanation would allow for the existence of 230-m-tall swales or ramparts if there were extensive mantling deposits encroaching upon the ejecta blanket. The image shown in Fig. 6 suggests that near-rim ice deposits, perhaps covered by dunes or a thin dust mantle, could be the cause of the unexpectedly tall ramparts within one crater radius of the rim. The exponent (b) in the ETF for this crater is -0.50, which is typical of many impact craters in the northern hemisphere of Mars (Garvin and Frawley 1998), but far removed from the mean value for polar region features.

FEATURE "D": COMPLEX ICE-FILLED CRATER AT 77°N, 215°E

A 44-km-diameter complex impact crater filled with high-albedo and essentially featureless cavity interior deposits is illustrated in Fig. 7 (crater D in Fig. 1). This impact structure is at least 2.1 km deep and possesses a rim with ∼0.98 km of relief relative to the surrounding preimpact surface (Table II). MOLA obtained an off-center pass on MGS orbit 242, which suggests that the infilling materials may be organized as a relatively uniform shelf, with a semicircular trough adjacent to the eastern portion of the crater's inner wall (Fig. 7). The expected depth for a crater of this diameter in the polar region of Mars is 1.54 km, while that estimated using the general relation for the northern hemisphere is 1.6 km. The crater in Fig. 7 is 500–560 m too deep, if the empirical scaling relationships presented previously are representative. As with the crater shown previously in Fig. 6, a multilevel crater floor deposit is observed, with the deepest part of the cavity localized in one region of the inner cavity wall. In spite of its "overdeep" status, over 460 km^3 of cavity infilling materials is estimated on the basis of model volumes and depths

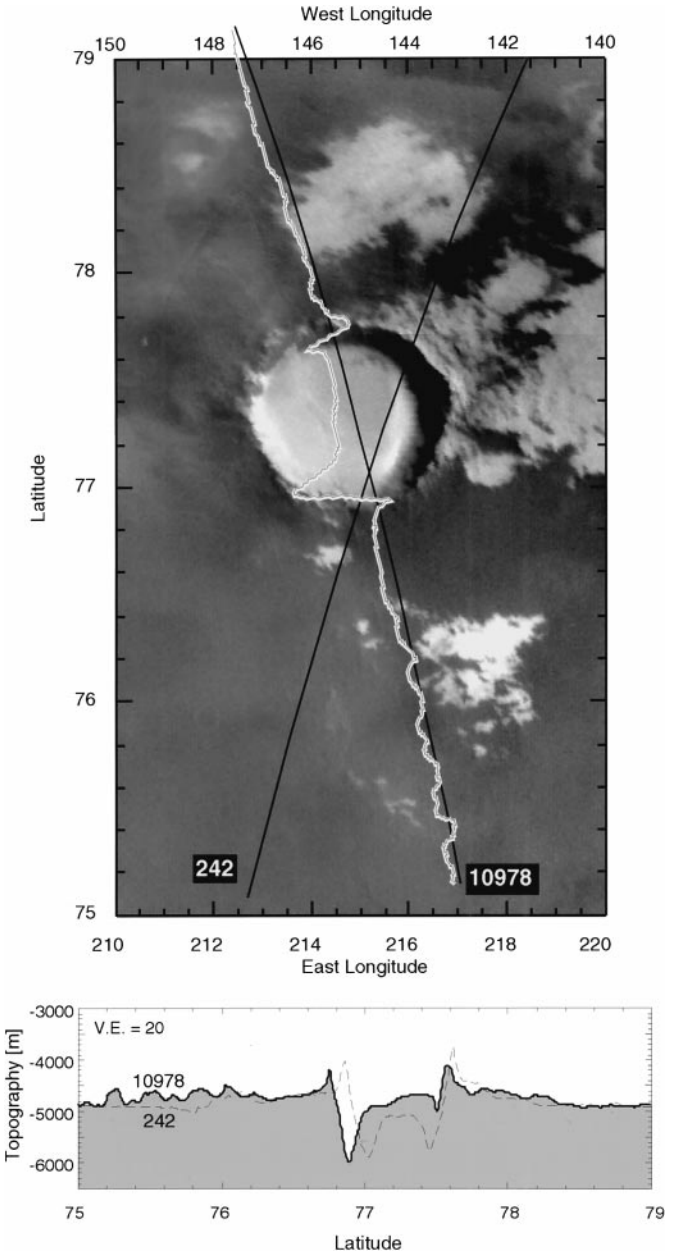

FIG. 7. Example of a 44-km-diameter crater located at 77°N, 215°E (Feature D in Fig. 1). A plug-like cavity interior deposit (as observed previously in Fig. 3) is indicated. White gaps are due to clouds. Note the 200-m relief of the ejecta ramparts at the south of the ejecta blanket.

(Tables II and III). Spread as a uniform layer over the ∼900 km^2 area of cavity floor, this volume would result in a layer thickness of ∼510 m. There is no longer a discrepancy between the observed depth from the rim crest (2.1 km) and the expected depth (1.54–1.59 km) if we consider the more than 500 m of uniform thickness infill as part of the floor. As with the example shown in Fig. 3, the cavity interior geometry is highly U-shaped ($n = 4.1$), with inner cavity wall slopes of more than 11°. This geometry, in combination with the 0.98 km of sharp rim relief, indicates that

this impact feature is not highly degraded. However, the amount of time required to accumulate more than 500 m of cavity fill is likely between $\sim 2 \times 10^6$ and 10^7 years (Thomas *et al.* 1992), assuming uniform sedimentation at less than 8×10^{-4} cm/year (Plaut *et al.* 1988). Even these timescales are relatively short in a martian geologic context. This analysis is based on the off-center MOLA pass on MGS orbit 242. Figure 7 also shows recent mapping pass 10978 that is through the crater center. The measured values are not substantially different, other than a slightly larger amount of apparent infill in the mapping pass.

The modeled volume of excavation for this crater (Fig. 7) is $\sim$700 km^3 in excess of the modeled final cavity volume (preerosion), not considering cavity slumping and other factors (Table II). This difference is larger than the estimated volume of infill ($\sim$460 km^3) but within 50%. Thus, we can explain the large levels of possibly ice-rich deposits in the interiors of several near-polar cap impact features as a consequence of continuous deposition over long time periods (i.e., tens of millions of years). A similar end result could be achieved if the polar deposition rate were episodically higher during times of polar cap radial advance, which could bury the cavities of smaller, less-deep impact craters. Larger craters such as the 44-km-diameter example shown in Fig. 7, would retain a significant fraction of this cavity fill, even after a long period of ablation. Smaller, shallower craters would retain less, which is consistent with observations for virtually all ice-associated impact features north of 72°N for which we have MOLA coverage (Tables II and III).

FEATURE "E": 80-Km-DIAMETER COMPLEX CRATER *KOROLEV* (73°N, 163°E)

Korolev is the largest north polar region impact crater (crater E in Fig. 1), with a diameter of $\sim$80 km. MOLA acquired only one SPO mission phase cross section that sampled the cavity of this important impact feature, on MGS orbit 332. Partial loss of data has made analysis of the geometric properties more difficult. Early MGS mapping mission coverage, however, has provided centerline MOLA transects of this impact feature. From a digital elevation model (DEM) constructed from numerous near-center and off-center passes, we find a maximum depth of 2.62 km and an integrated volume of 6500 km. Figure 8 illustrates *Korolev* and the best MOLA cavity cross-section (pass 10146) through the center of the crater currently available. In this pass, *Korolev* exhibits a 0.91-km rim, relative to the surrounding preimpact surface, and a total depth of 2.2 km, which is approximately equal to or slightly deeper than that estimated from polar region depth–diameter scaling relationships. Maximum depth derived from the DEM is $\sim$0.240 km less than that estimated from polar region depth–diameter scaling relationships. This would suggest that its cavity is infilled to a uniform level of 0.24 km. However, the high-resolution Viking image inset (Fig. 8) indicates that there is considerable cavity floor texture (i.e., escarpments as observed at the crater in Fig. 4), and the MOLA topographic data displays about 1 km of floor relief variability. This crater is one of the relatively oldest in the northern high latitudes on the basis of a number of 5- to 10-km-diameter impact features that can be observed within one crater diameter of its rim crest, superimposed on the continuous ejecta blanket (CEB).

The average ejecta thickness within the CEB in this pass is 123 m, on the basis of the effective surface area of this deposit and its MOLA-based relief. In comparison, the mean ejecta thickness (CEB) for the 44-km impact feature displayed in Fig. 7 is 124 m, while that for the 19-km crater (Fig. 3) in Olympia Planitia is 43 m (Table III). The latter value would suggest that some burial of the *Korolev* ejecta has occurred, which could also explain the relatively low relief (0.78–1.04 km) of its rim region. For comparison, the 95-km diameter impact crater known as *Mie*, located at 48°N, 139°E, displays a rim relief of $\sim$1.1 km, in spite of obvious rim burial effects.

The disparity in the model cavity depth (2.86 km) calculated from the DEM average diameter of 80 km and the apparent maximum DEM depth (2.62 km) could be attributed to sampling bias. The MOLA transect (Fig. 8) is a centerline pass, but the floor depth is clearly locally variable. If we consider the apparent depth of the centerline pass (2.2 km) in Fig. 8, however, to be representative, then more than 600 m of infill would be required to explain the disparity in depths. Moreover, the difference between the model cavity volume (7800 km^3) and the apparent volume from the DEM ($\sim$6500 km^3) is 1300 km^3, which is equivalent to a uniform layer of thickness $\sim$0.40 km across the entire floor of the crater. It would require between 15 and 60 Ma to accumulate $\sim$400 m of infill and three times longer to develop a level of infill as thick as 1.5 km, which is the maximal relief of the central deposits within the cavity. We can conclude only that high sedimentation rates, on the average, are required in the northern high latitudes to explain our MOLA observations. This is consistent with the apparent levels of burial and cavity interior infill at *Mie* crater (48°N).

Figure 9 summarizes MOLA topographic observations at a common scale for the four distinctive ice-filled craters examined to date (Figs. 9A, 9B, 9C, and 9D are Features "B", "A", "D", and "E", respectively). Each has been discussed above as case examples (Figs. 3–8). For each structure, we have indicated the topographically defined rim, and the approximate continuous ejecta extent from topography and images. The 34-km crater (Fig. 9A) cavity is filled to more than 80% of its model cavity volume and depth. Its rim remains as the most readily identifiable crater feature (see also Fig. 4). Figure 9B is the 19-km-diameter impact feature in the Olympia Planitia dune field from Fig. 3. Figures 9C and 9D are the 44-km-diameter crater from Fig. 6 and *Korolev* crater from Fig. 8, respectively. On the basis of the voluminous infill deposits inferred from topology (MOLA) and morphology (Viking images), average crater floor deposit thickness for each of these features varies considerably (Table III): 710 m for the crater in Fig. 9A, 295 m for that in Fig. 9B, 514 m for that in Fig. 9C, and $\sim$400 m for that in Fig. 9D.

We can consider the mean ejecta thickness (Table III) for ice-associated impact craters as defined by the ratio of ejecta

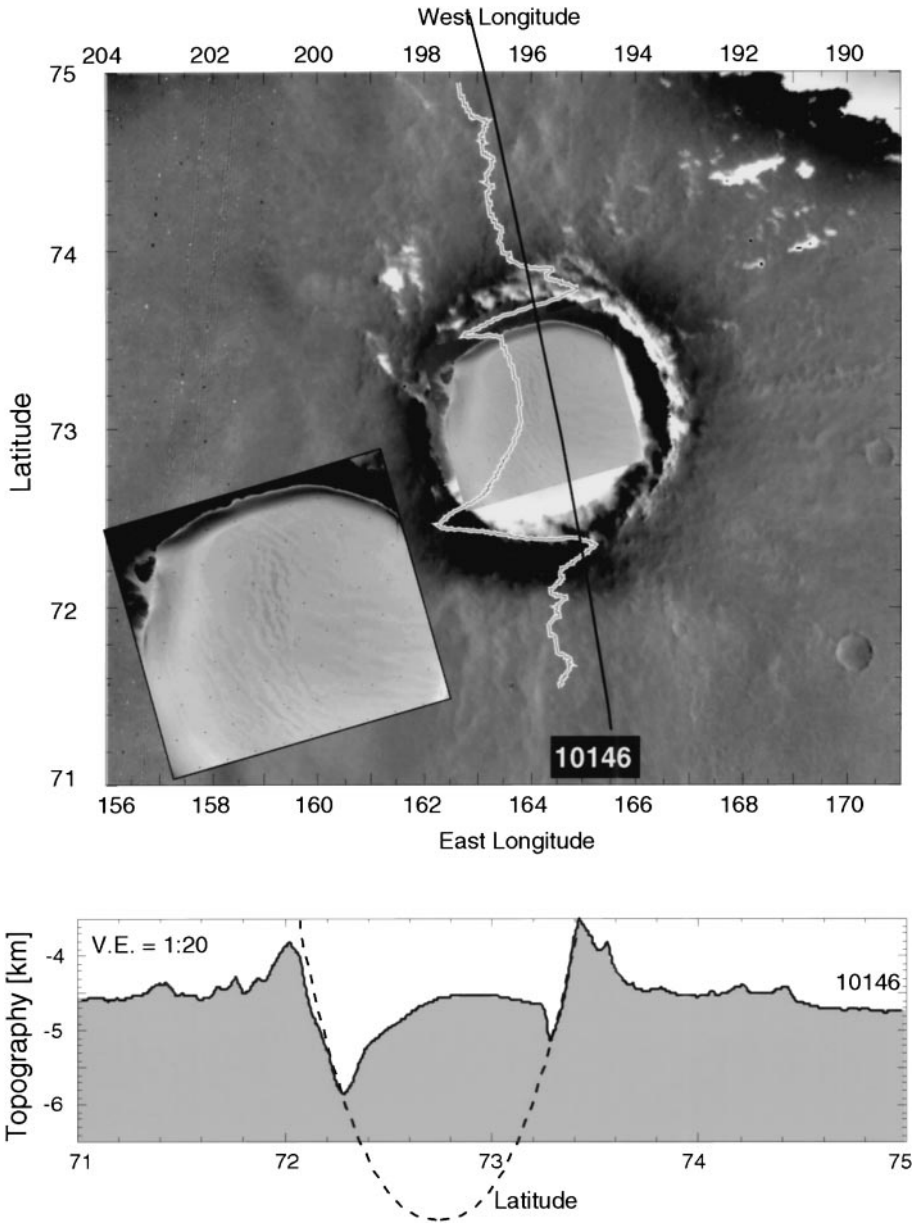

FIG. 8. 80 km crater *Korolev* located at 73°N, 163°E (Feature E in Fig. 1). MOLA's best cavity cross section for this crater was acquired during the early MGS mapping phase (mapping orbit 146). (Inset) A high-resolution Viking image that features the cavity floor. Curvilinear features similar to those observed at the crater in Fig. 4 are suggested.

volume to ejecta surface area. The four examples illustrated in Fig. 9 are noteworthy. The crater in Fig. 9A has a mean ejecta thickness of 52 m, while the crater within the Olympia Planitia dunes (Fig. 9B) displays a mean ejecta thickness of 43 m. The two largest impact structures (Figs. 9C and 9D) display average ejecta thicknesses of 124 and 123 m (*Korolev*), respectively. The crater shown previously in Fig. 6 suggests a mean ejecta thickness of 54 m, within 1–2% of that of the crater in Fig. 9A). Of all of the ice-associated impact features considered in this investigation (Table II), only the two largest (Figs. 9C and 9D) demonstrate average ejecta thickness values in excess of 120 m.

FEATURE "F": CRATER ON MARGIN OF POLAR CAP RESIDUAL ICE (81°N, 255°E)

Table II displays the salient geometric properties of several additional impact craters associated with ice or frost. MOLA first traversed one crater within the margin of the polar ice cap as part of MGS orbit 208. Figure 10 illustrates this ice-margin impact feature (crater F in Fig. 1) and two MOLA topographic cross sections that sampled its central cavity (MGS orbits 1666 and 10750). This ice-bound crater is only 18 km in diameter, with a depth–diameter (d/D) ratio similar to those of other North Polar

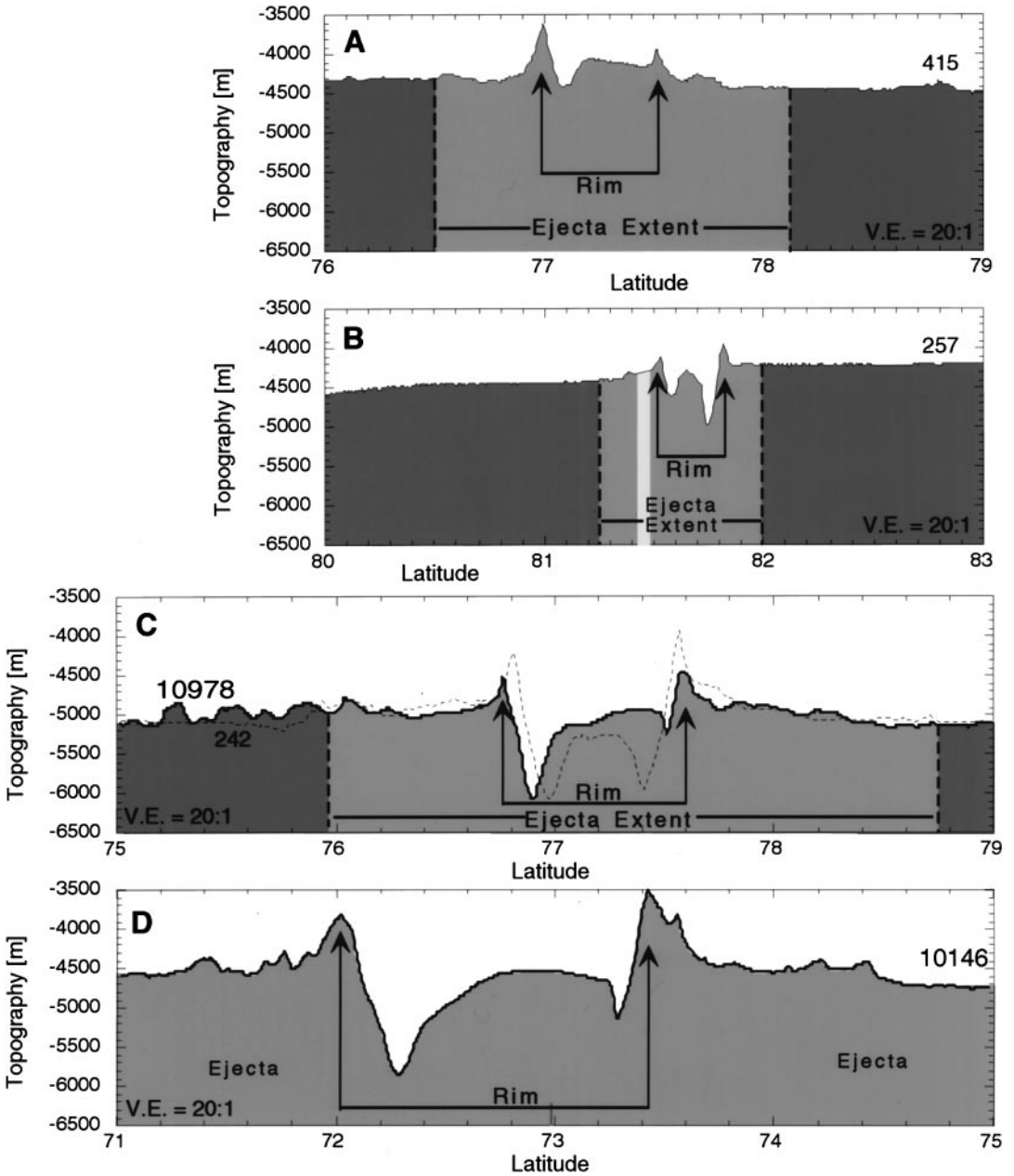

FIG. 9. Comparison of MOLA cross sections for craters illustrated previously in Figs. 3, 4, 7, and 8. (A) Crater shown in Fig. 4. (B) Crater shown in Fig. 3 (in *Olympia Planitia*). (C) Crater shown in Fig. 7. (D) Crater shown in Fig. 8 (*Korolev*). Rim crests are indicated by arrows and ejecta extent, as defined on the basis of MOLA topography and Viking images is indicated by dashed lines. MGS orbit numbers are shown at right. See text for details.

Region impact craters (0.034). What makes it unique is its cavity, whose inner walls feature average slopes less than or equal to 5.0°. Aside from *Korolev*, all of the high-latitude impact features observed by MOLA display inner cavity wall slopes that average greater than 9–10°. In addition, its average rim height (Table II) is the lowest observed of any of the ice-associated craters. Table III illustrates its uniqueness in terms of a computed infill thickness. This ice-margin crater displays 430 m of apparent cavity infill, which is within 100 m of the thickness of the margin of the north polar ice cap in this area (Fig. 10). The model depth of excavation for this is ∼1.5 km, suggesting that the impact may have excavated sub-ice cap basement materials. The average rim height for this crater is only 110 m, at least a factor of two under what would be expected. We attribute the anomalously shallow depth and low-relief rim of this crater to ice-related modification processes. It would require 14 to 60 million years to accumulate 430 m of infilling deposits in a crater such as this at typical polar sedimentation rates. If one invokes the maximum rates (30 m per 100,000 years) computed for Mars (Thomas *et al.* 1992), one could fill the cavity of the crater illustrated in Fig. 10

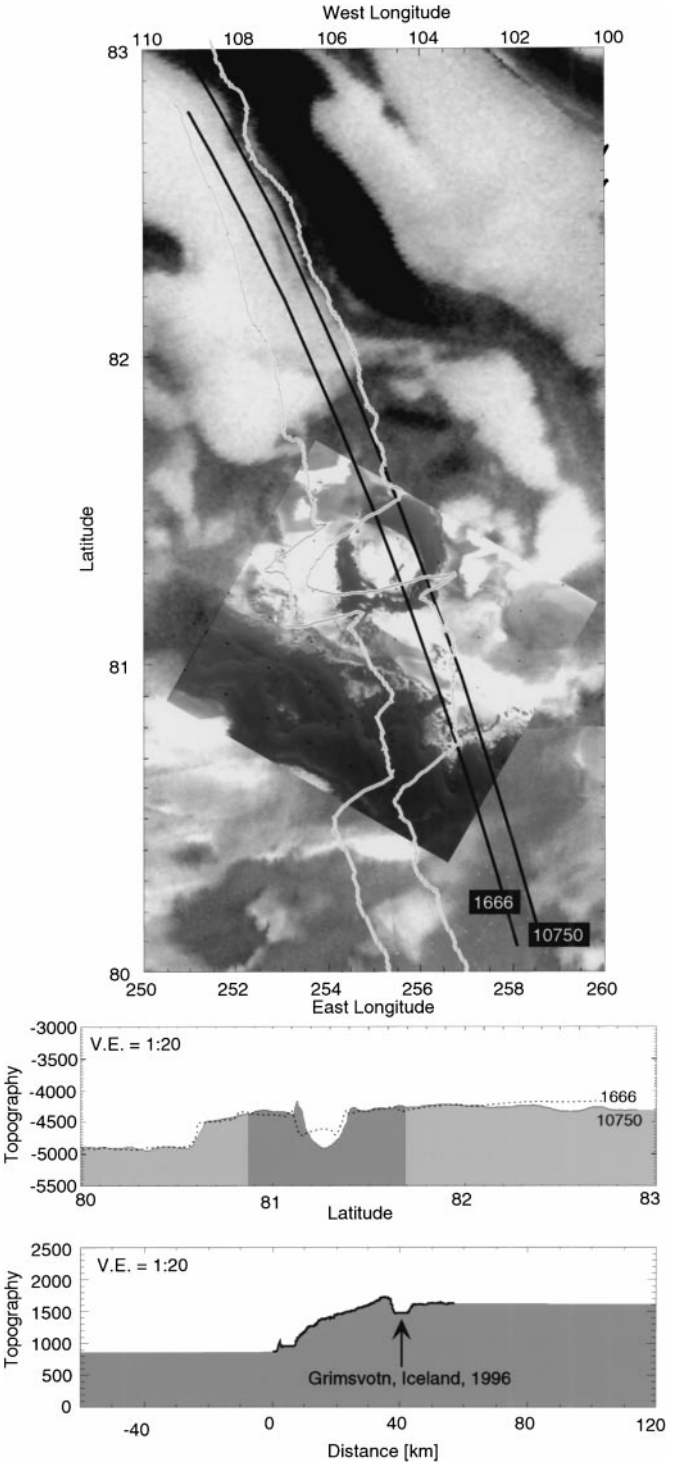

FIG. 10. Example of an 18-km-diameter crater located on the margin of the North Polar Cap at 81°N, 255°E (Feature "F" in Fig. 1). (Bottom) A NASA aircraft laser altimeter cross-section (W to E) across the ∼10-km-diameter *Grimsvotn* subglacial caldera in the *Vatnajokull* ice cap of Iceland. The data have been thinned to approximate the MOLA sampling. *Grimsvotn* shows higher cavity wall slopes than the martian impact crater but similar cavity geometry. See text for details.

in ∼1.4 million years. Improved images (i.e., from MOC) are needed to constrain the morphologic evolution of this crater in the marginal ice of the north polar cap.

We have compared the crater shown in Fig. 10a with a ∼10-km-diameter volcanic crater that formed in the *Vatnajokull* ice cap of Iceland. This feature (Fig. 10c) is the site of the most active subglacial volcano on Earth: *Grimsvotn*. Its geometrical properties are dynamic (Gudmundsson 1989), and a recent eruption (December 1998) has further modified its morphology. *Grimsvotn* displays a variable relief rim region, a topographically changing floor, and cavity wall slopes (10–16°) similar to the martian crater illustrated in Fig. 10a. *Grimsvotn* was formed and maintained in a terrestrial ice cap between 250 and 500 m in thickness (Gudmundsson 1989) by subglacial volcanism. The impact that formed the 18-km-diameter crater at 81°N, 255°E on Mars may have generated up to ∼1.7 km^3 of impact melt in the floor of a crater that was once 0.8 km in depth. The residence time of this volume of melted materials (i.e., assuming they are silicates) is on the order of 10,000 years. Whether a short-lived period of impact-induced sub-ice-cap melting could have sustained a fresh cavity geometry (i.e., *Grimsvotn*-like) on Mars is uncertain. However, with further MOLA observations, it may be possible to model the three-dimensional topology of impact craters in the ice and compare them more closely with possible terrestrial analogs such as the *Grimsvotn* caldera.

FEATURE "G": ICE-ASSOCIATED CRATER AT 77°N, 195°E

Another well-sampled (by MOLA) ice-associated crater was traversed on MGS orbit 240 (Fig. 11). Tables II and III summarize the geometric properties for this 20-km-diameter feature (crater G in Fig. 1). The apparent depth of infill at this crater is similar to that of the crater located at 82°N, 190°E within the Olympia Planitia dunes (Fig. 3 and Feature "A" in Fig. 1). Figure 11 illustrates low-albedo dune materials associated with the crater cavity and high-albedo residual ice deposits north of the crater and on the north-facing cavity wall slopes. A smaller dune-mantled crater barely visible in the Viking images appears to be located within the continuous ejecta blanket and just south of the crater rim. Many of the characteristics of this moderately eroded 20-km polar impact feature are similar to those for the crater illustrated in Fig. 3, with the exception of cavity floor deposits. The MOLA pass of this crater (Fig. 11) exhibits no topographic signature of the dome-like central deposits or multilevel cavity interior deposits discussed previously for craters of this size. It is possible that the location of this crater, just south of the edge of the Olympia Planitia dunes, has affected its cavity geometry. If weak or easily mobilized (i.e., ice-rich) target materials were not involved in the impact that formed the crater shown in Fig. 11, then its cavity may have evolved in a more traditional manner. The parabolic cavity shape observed for the crater in Fig. 11 is consistent with most 20-km scale

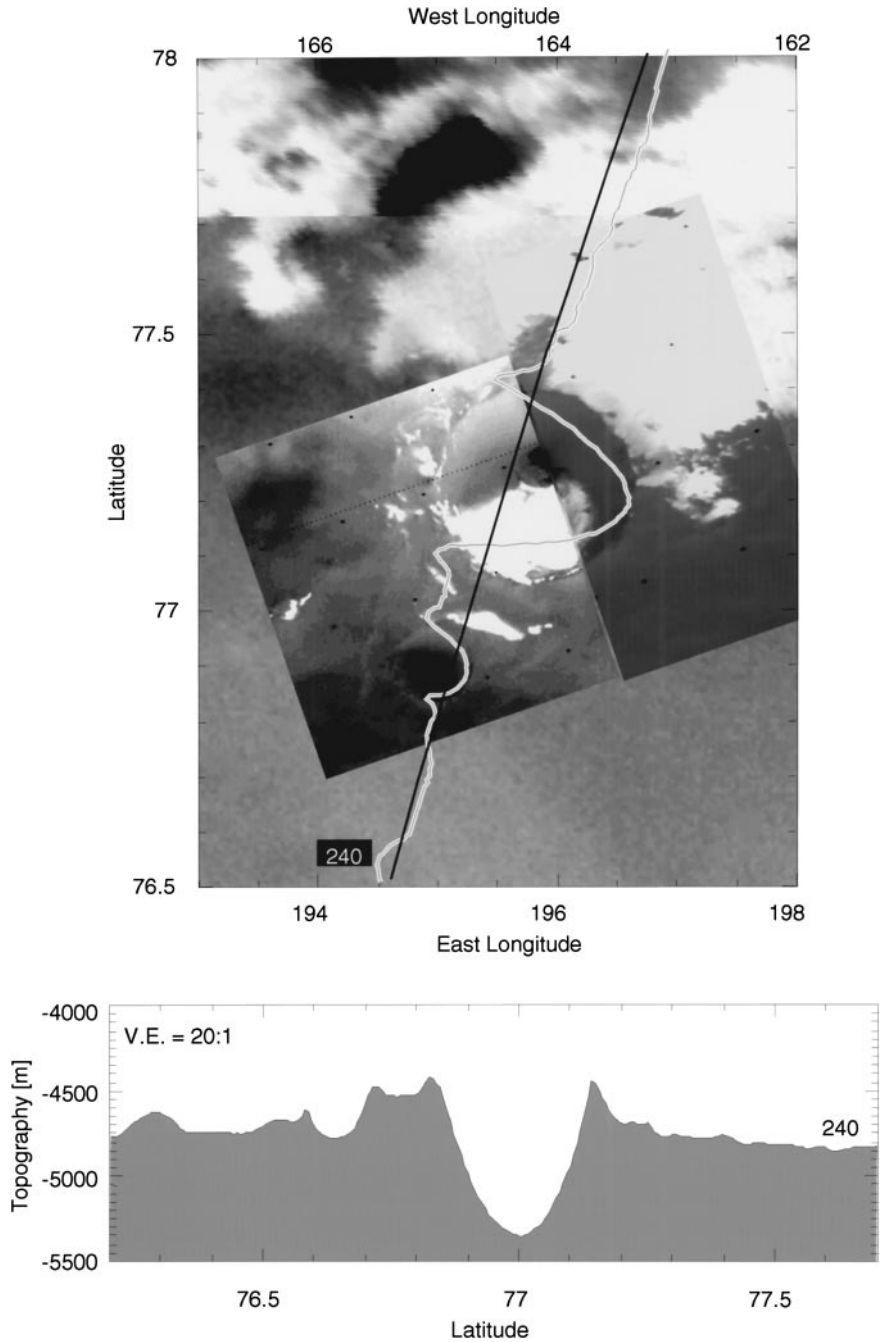

FIG. 11. Example of a 20-km-diameter crater located at 77°N, 195°E (at edge of *Olympia Planitia* dunes, Feature G in Fig. 1). This feature is located a few hundred kilometers from the crater shown in Fig. 3. Ice or frost associated with north-facing slopes is indicated by the Viking image.

impact features on Mars, as sampled by MOLA (Garvin and Frawley 1998).

FEATURE "H": ICE-ASSOCIATED CRATER AT 79°N, 62°E

Figure 12 illustrates an 18-km-diameter crater associated with outlier ice deposits (crater H in Fig. 1). Two SPO passes within 10% of the centerline were used to measure the information in Table II. These did not completely sample the assymetric deposit, so two recent centerline MOLA cross sections, acquired on MGS Orbits 10978 and 11763, are shown in Fig. 12 and allow us to consider its cavity geometry in comparison with other examples. As with the craters in Figs. 3, 7, and 11, this feature displays substantial off-center (>600 m) cavity interior deposits. While these are less than the major deposits observed at the crater shown in Fig. 3, its relative levels of infill are consistent with other north polar region craters in this diameter interval.

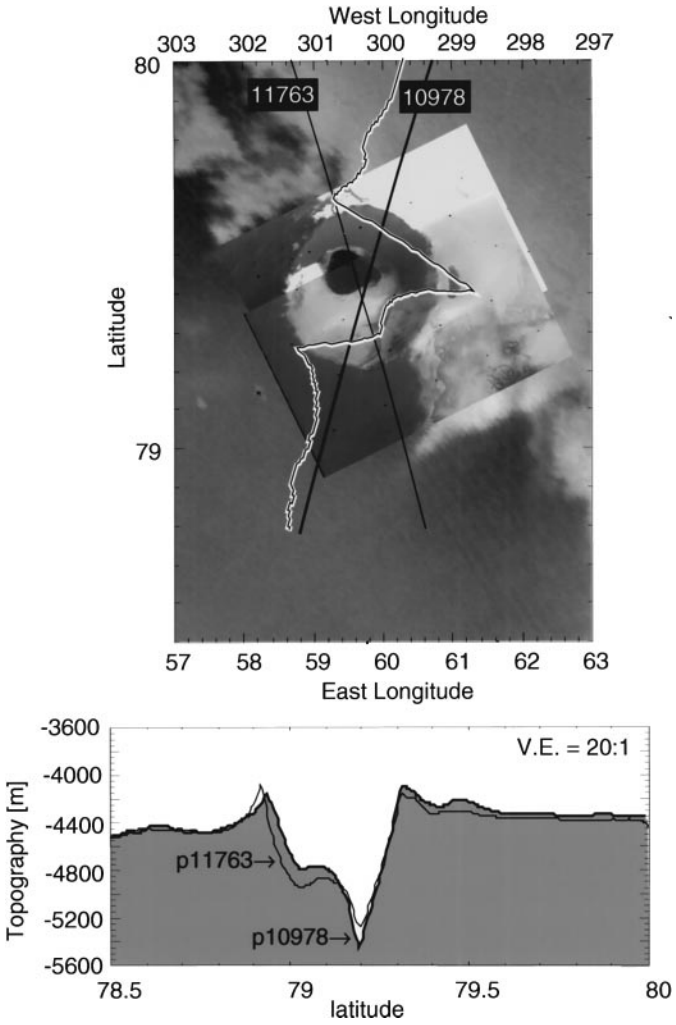

FIG. 12. Example of an 18-km-diameter crater located at 79°N, 62°E (Feature H in Fig. 1). This crater displays 100- to 150-m-scale ramparts that are barely discernible in the Viking image.

FEATURE "I": NEAR-ICE CRATER LOCATED AT 72°N, 345°E

A 20-km-diameter crater located adjacent to outlying deposits of ice is illustrated in Fig. 13 (crater I in Fig. 1). This well-preserved impact feature displays a lobate ejecta blanket with marginal ramparts and polygonal planform geometry. Its apparent depth is 1.47 km, which is within 200 m of the model depth of excavation for a 20-km crater on Mars. A near centerline MOLA cross section (Fig. 13) clearly illustrates the classic topographic elements of this fresh-appearing complex crater. Its continuous ejecta blanket, away from the near rim region, is concave, terminating in a rampart over 100 m in relative relief. The apparent cavity volume for this 20 km diameter crater is 215 km^3, or nearly two times greater than the other craters observed by MOLA in this diameter size class. The apparent crater depth exceeds that which would be predicted by MOLA or theoretical scaling relationships by almost 400 m. A small central deposit on the crater floor is observed, with ∼200 m of relief. The absolute cavity floor elevation of this crater (Table II) is within 150 m of the lowest crater floor elevation observed for the highest northern latitudes. It appears to have escaped any major infilling episodes, perhaps because of its larger distance from the margin of the polar cap relative to the other ice-associated craters discussed here) or because of its extreme youth.

FEATURE "J": MULTILOBE EJECTA CRATER AT 73°N, 38°E

In contrast, the crater illustrated in Fig. 14, is a fresh, multilobed impact feature not associated with any evidence of ice or frost deposits (crater J in Fig. 1). It is 9 km in diameter with an apparent depth of 1.03 km. The Viking Orbiter image in Fig. 14 suggests that it may contain a small central mound, but the MOLA cross-section did not sample this feature. Two series of ramparts (ejecta lobes) can be observed. Inner cavity wall slopes are typically 20° at this feature. Its rim averages 320 m in relief, larger than is typical of Northern Hemisphere craters on Mars in general (Garvin and Frawley 1998). Its cavity is nearly paraboloidal, and its ejecta extends more than four crater radii from the rim. The difference between the apparent depth (1.03 km) and the model depth of excavation (0.85 km) for this feature is positive. This means that the crater is too deep by over 180 m relative to the general model for excavation for Mars (Barlow and Bradley 1990). This could be explained only if the excavation were more efficient than would be anticipated due to target strength effects. The two craters illustrated in Figs. 13 and 14 are the furthest from the polar cap of those discussed in this paper and show minimal association with ice deposits within their cavities, but could have excavated into ice-rich target materials. The 0.85-km depth of excavation for the 9-km crater at 73°N, 38°E (Table III) could have reached a locally shallow groundwater or ground-ice table as suggested by Clifford (1993), and enhanced cavity formation and ejecta emplacement would be one result. From the ejecta topology provided by MOLA (Fig. 14), it appears that the radial, lobate ejecta deposit originates from the outer base of the rim uplift region and builds ramparts that are up to 150 m in relief, with secondary, distal ramparts with 50 m of relief. Additional MOLA samples of such multi-lobed or fluidized-ejecta impact craters are needed to more fully develop a physical model for the ejecta emplacement (Garvin and Baloga 1999).

FEATURE "K": CRATERFORM AT 78°N, 293°E

A 7.3-km-diameter craterform that appears to be located at the summit of a low-relief cone is illustrated in Fig. 15 (crater K in Fig. 1). The basal diameter of the low-relief martian cratered cone (MCC) is ∼19.5 km, with a total height of 444 m, relative to the regional background. A long-wavelength (∼80 km) topographic sag with a vertical magnitude of ∼60 m is associated with the MCC. This feature displays high-albedo "ice" deposits on all north-facing slopes. The typical slopes associated with the

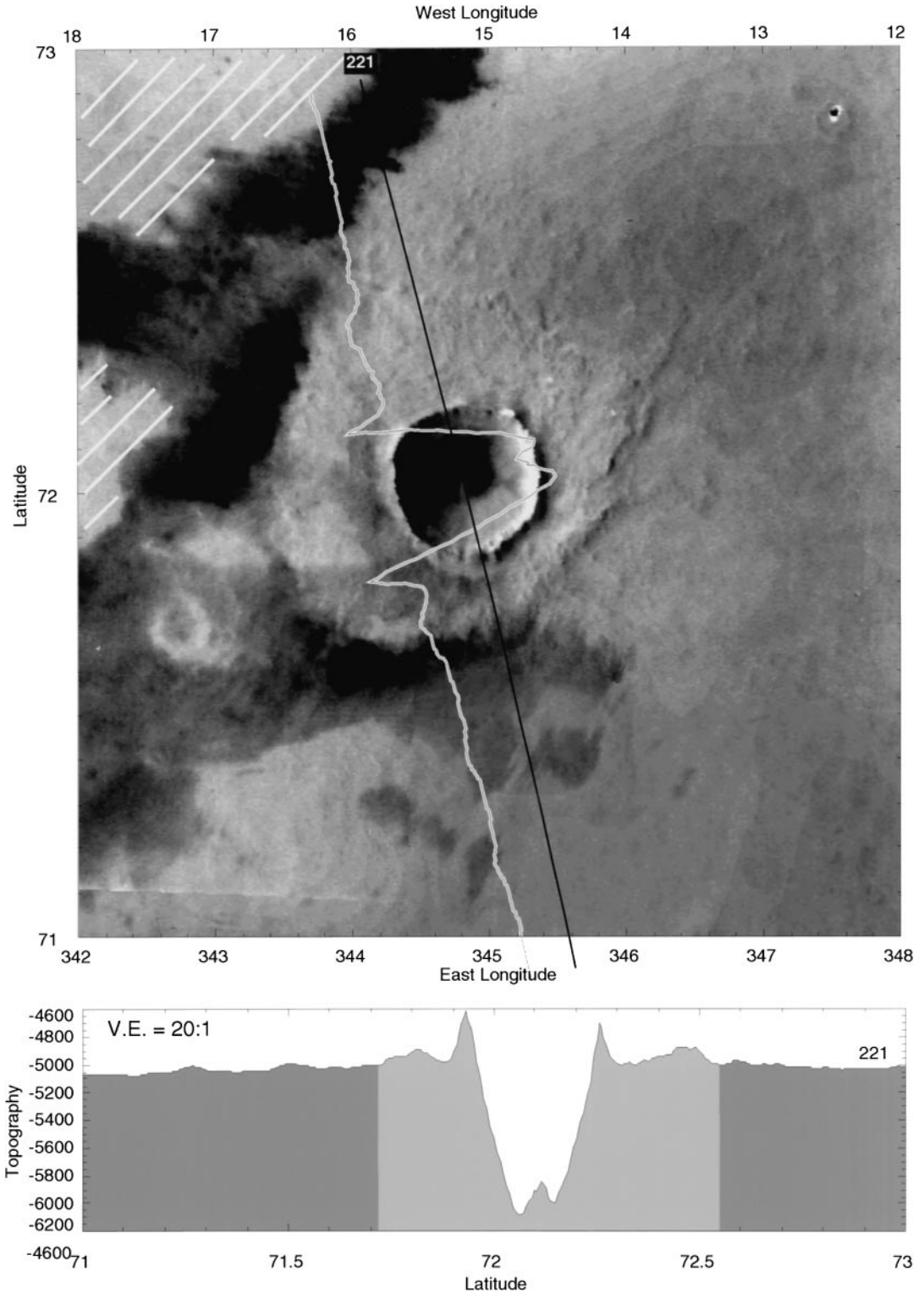

FIG. 13. Example of a 20-km-diameter crater located at 72°N, 345°E (Feature I in Fig. 1) adjacent to outlying ice deposits (hatched areas at left in the image). This fresh-appearing crater displays a small central deposit covered by low-albedo dune materials and 100-m-scale (vertical) ramparts. This crater is 1.47 km deep.

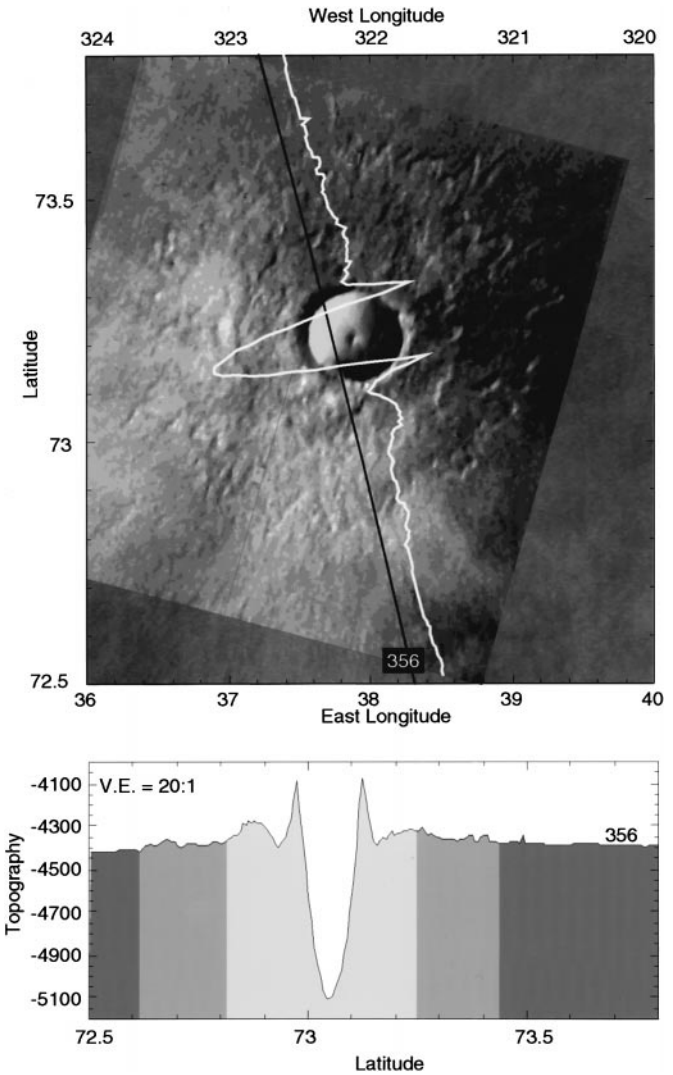

FIG. 14. Example of a fresh-appearing 9-km-diameter multilobed ejecta crater located at 73°N, 38°E (Feature J in Fig. 1). There is no indication of any ice or frost association for this transitional geometry feature. This crater has an apparent depth (from MOLA measurements) that is in excess of its expected depth of excavation.

conical part of this landform are 3.8° to 6.0°. Slopes associated with the inner walls of the summit crater cavity are typically 4°, and the crater cavity has a conical shape ($n = 1.4$). From these simple geometric properties, and because the crater cavity floor is ∼250 m above the level of the surrounding surface, we conclude that this MCC feature represents a volcanic edifice. Hodges and Moore (1994) ascribed this feature to water–magma interactions such as are associated with maar volcanism on Earth. The flank slopes (∼4.0°), the ratio of flank to cavity slopes (1.2), and the geometric properties of the summit crater, for this feature are all consistent with low-relief lava shield volcanoes found on Earth in subpolar environments. Indeed, Garvin and Williams (1990) described the lava shields of Iceland in terms of parameters such as flank slope, areal productivity (edifice volume V divided by basal diameter D: V/D), and cross-sectional shape (n). The feature illustrated in Fig. 15 most clearly resembles the low-relief lava shields of Iceland in its geometric characteristics. Such landforms display flank slopes in the 3–5° range and have V/D values between 0.65 and 1.5 (Garvin 1996, Williams *et al.* 1983, Garvin and Williams 1990). We can find no reason to require hydromagmatic volcanism to construct a low-relief edifice such as that illustrated in Fig. 15. Indeed, on Mars, maar style volcanism, if present, would be expected to favor the formation larger, steeply sloping craters than conical features whose flanks average a few degrees in local slope (Mouginis-Mark *et al.* 1992, Wilson and Head 1994). Other non-impact-related craterforms have also been observed in the north polar region of Mars

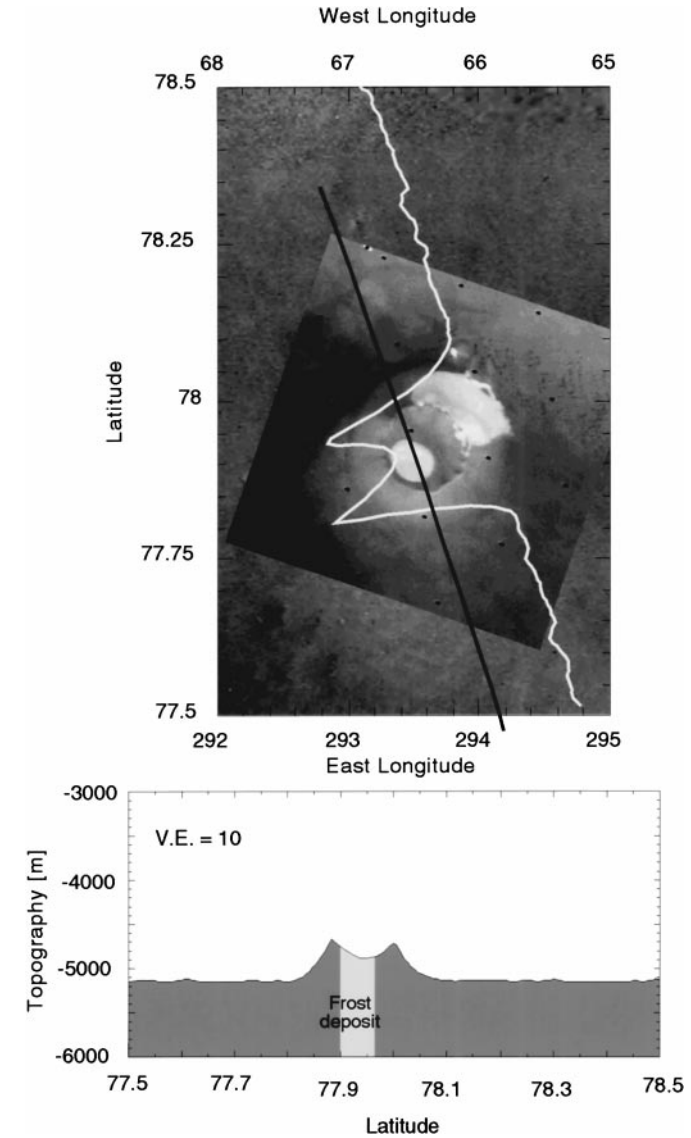

FIG. 15. Example of a 20-km-diameter (base) martian cratered cone (MCC) located at 78°N, 293°E (Feature K in Fig. 1). The 7.3-km-diameter crater atop this low-relief cone is unlike any impact craters traversed by MOLA. See text for details.

(Hodges and Moore 1994), but incomplete MOLA sampling makes quantitative analysis uncertain at this time.

Table II includes an entry for a crater-like feature at the head of *Chasma Boreale*. This 11-km-diameter landform was not imaged with adequate resolution by the Viking Orbiters to assess its mode of origin. A near-centerline cross section of the feature was acquired by MOLA on MGS orbit 208. From this profile, we have noted its depth (1.08 km), "cavity" wall slopes (16°), cavity shape ($n = 1.2$), and other parameters (Table II). From every indication, this feature could represent another ice-margin impact feature, similar to that discussed previously (Fig. 10). The apparent rim relief (110 m) is similar to the ice-margin crater illustrated in Fig. 10. However, if this craterform is of impact origin, the steepness of its cavity walls, its elevated depth–diameter ratio (0.10), and large depth, relative to a similarly sized crater (i.e., Fig. 10), would suggest that it is geologically recent (<1–10 Ma). Without additional MOLA cross-sections and MOC images, however, an unambiguous interpretation is not possible at this time. From analysis of cross-sectional shape of the spiral canyons and troughs in the north polar cap of Mars (Zuber *et al.* 1998), it is not likely that the *Chasma Boreale* "crater" located at 85°N, 2°E is a typical ice cap feature.

DISCUSSION

Our preliminary synthesis of a population of north polar region impact craters on Mars using newly acquired MOLA topographic measurements provides new insights into the characteristics of this area. We have considered several aspects in this paper, mostly focused on simple geometric parameters. Our discussion treats each of these in order.

Impact crater depth-to-diameter ratios provide first-order information on both target properties and postimpact degradation processes. We have explored d/D values measured for polar region impact craters in comparison to those observed for nonpolar latitude examples. MOLA measurements of this parameter are more sensitive to topographic subtleties than most previous measurements on the basis of the high vertical precision of the instrument. The mean depth-to-diameter (d/D) ratio for polar region craters is 0.035 ± 0.02, while that for nonpolar region impact features is 0.053 ± 0.04. These differences are significant because the sample populations involved are greater than 100 in each case. However, the sampling achieved by MOLA to date is not randomly distributed and there will be a bias associated with the improved sampling statistics for higher latitude craters simply on the basis of orbital geometry (Zuber *et al.* 1998). With periapsis for the MGS in the vicinity of the north polar cap, denser sampling was achieved for those latitudes north of 50°N.

The crater cavity volume measurements demonstrate that polar crater cavities are volumetrically larger than those in other regions, and that for crater diameters larger than ~52 km, the polar crater cavity volume is always greater than it is for craters at lower latitudes. This is perhaps a consequence of target properties such as an increase in abundance of volatiles or unconsolidated sediments that enable enhanced excavation at high kinetic energies. Indeed, the apparent effect on crater cavity volume of polar target properties appears to change with increasing diameter such that the largest complex craters are less distinctive from their equatorial counterparts. For crater cross-sectional cavity shape, the polar and nonpolar power laws relating cavity shape and crater diameter suggest that there is a strong tendency for craters to become more paraboloidal with increasing diameter, independent of location.

Fresh impact crater cavity depth is a reasonable proxy for target mechanical properties. Ice-associated craters in the north polar region are frequently extraordinarily deep (Tables II and III). In these cases, the evidence supports enhanced excavation of what appears to be a weak target. Such impact features demonstrate apparent cavity depths that either come close to or exceed the model depth of excavation for general martian impact craters. The simplest explanation calls for a target that enables enhanced excavation, without subsequent modification (fall-back, slumping) to preserve large apparent cavity depths. A weak layer, buried less than several hundred meters, and spatially extensive is one possible explanation. In this case, final excavation for smaller impact craters would involve the weaker layer, enhancing final crater depth. We are continuing to investigate whether excavation into a subsurface ice target would adequately explain the observations presented herein.

We have considered impact crater rim height in our measurements. However, while the trends for rim height appear to follow those for crater depth, there is greater uncertainty. This is because most of our existing (pre-MGS mapping) measurements have been derived from one or two cavity-crossing MOLA profiles. Such profiles do not adequately sample the variability of rim height for most martian craters. Early MOLA mapping results (Garvin *et al.* 1999) suggest that mean rim height is highly correlated with cavity depth for fresh craters.

The mean and modal values of the ejecta thickness function (ETF) exponent for both polar and nonpolar craters are outside of the previously described acceptable range (-2.5 to -3.5) as suggested by Melosh (1989). We suggest that this is likely the result of a dependence of ejecta topology on latitude (and hence target type), but as yet, the large variability and insufficient statistics in our measured ETF distribution allows little further speculation.

For the ratio of ejecta volume to cavity volume (V_{ej}/V), we find that the ratio is larger for polar craters than for nonpolar craters. We suggest from the combination of MOLA topographic cross-sectional and Viking images that there is ample evidence of significant levels of cavity infill in the highest northern latitudes of Mars that can be quantified by MOLA topographic data. The infill volumes contribute significantly to the apparent increase in V_{ej}/V due to the artificial lowering of the cavity volume term (V) in this parameter. In addition, there is topographic evidence of ejecta burial for some of the larger polar region craters. Thus, we must use extreme care when interpreting the emerging pattern in this volume ratio parameter until two-dimensional digital

elevation models (DEMs) from large numbers of MOLA transects can be constructed and used to reconstruct cavity geometries.

The elevation of impact crater floors can be used as a regional indicator of upper crustal structure. The high vertical accuracy of MOLA topographic data makes it ideally suited for examining crater floor elevations within specific regions on Mars. The absolute elevation of the apparent crater floor at *Korolev* is −6250 m, which is only 250 m lower than that of the 44-km feature at 77°N, 215°E (Table III). Other high-latitude impact structures in the 75- to 100-km-diameter size interval, including *Mie* (48°N) and *Lomonosov* (65°N), display average floor elevations between −6500 and −6700 m, within 500 m of that measured for *Korolev*. On the basis of MOLA data, it appears that all of the larger complex craters in the northernmost Northern Hemisphere have floor elevations within about 500–700 m of one another. This tight clustering of surface elevations within a region as large as Antarctica on Earth could well be the consequence of limited sampling statistics. On the other hand, if there were a consistent floor elevation associated with a significant number of the largest polar complex craters, it could indicate a common level of regional sedimentation, as is typical of fluid-emplaced deposits on Earth (Smith *et al.* 1998, Craddock *et al.* 1997). It could also be linked to the thickness of a high-latitude sedimentary layer of low strength that overlies a more competent basement horizon. Excavation depths for craters 70 to 100 km in diameter are predicted to be in the 4.8- to 6.6-km interval, certainly adequate to excavate beneath any megaregolith layer and possibly to intersect the putative global groundwater system suggested by Clifford (1993). The similarity of cavity floor elevations for the largest complex craters on Mars may relate to excavation depths and hence to the stratigraphy of the upper 6 km of the martian crust in the north polar region.

A variety of crater-like features associated with ice, or located adjacent to the permanent north polar cap of Mars have been analyzed on the basis of MOLA topographic cross-sections in correlation with Viking Orbiter images. In several cases, ice-associated impact craters clearly display voluminous cavity interior deposits. Such deposits could require tens of millions of years to develop at the enhanced polar sedimentation rates suggested in Thomas *et al.* (1992) for layered bands. Episodic sedimentation, perhaps triggered by the advance of the polar ice cap, could explain the observed cavity infill volumes and thickness levels as measured by MOLA. However, this scenario would require enhanced sedimentation and subsequent minimal erosion of cavity infill deposits, to maintain the thickness levels required. A model in which the near-polar impact crater cavities are buried by ice/dust deposits and subsequently exhumed could also be invoked to explain some of the topographic features observed at ice-associated craters. In addition, those polar impact craters that appear to have excavated through the Olympia Planitia dune deposits demonstrate anomalous cavity interior deposit topologies, often suggesting a plug-like geometry (Fig. 3). Such features could be caused by enhanced melting in the cavity floor region, permitting large amount of interior fill deposits to form rapidly after crater formation, followed by slow erosion within a sheltered, closed depression.

Craters were observed in the marginal portions of the north polar cap (Garvin *et al.* 1998), as well as within the ice cap interior (Sakimoto and Garvin 1999). In at least one case (Fig. 10), a well-preserved crater appears to have been infilled by processes that have also attacked its rim. Whether the large level of cavity interior deposits required (430-m-thick layer) is caused by enhanced sedimentation or ice-related cavity wall slumping is unclear. Another candidate impact feature located at the margin of the ice cap near the head of *Chasma Boreale* appears to have an unmodified cavity depth, possibly attesting to its geologic youthfulness.

Martian craterforms associated with low-relief cones were also observed by MOLA. In at least one instance, a cratered cone located 120 km from the permanent ice cap (Fig. 1) most strongly resembles (in a geometric sense) low-relief terrestrial shield volcanoes rather than explosive volcanic craters associated with magma–water interactions. We suggest that this feature (Fig. 15) is a relatively recent basaltic lava shield volcano, with a low aspect ratio summit collapse crater. The formation ages of most of the craterform features observed in the north polar region appears to be less than 100 Ma and many could have been constructed in the past 1–10 Ma if sedimentation rates as high as 30 m per million years are regionally representative.

The observations summarized above offer several new interpretations of the target materials in the north polar region of Mars. Many questions remain, however. This preliminary analysis of a sample of high-latitude craterforms on Mars has provided a quantitative perspective on the volumes, slopes, and shapes of these commonplace features. It will hopefully serve as a frame of reference against which upcoming MOLA (and other MGS instruments) observations of the south polar region can be compared and contrasted.

ACKNOWLEDGMENTS

We gratefully acknowledge the strong support of the MOLA PI, Dave Smith, and the Deputy PI, Maria T. Zuber, in this work. We further acknowledge the support of the MGS Project at JPL who have operated the MGS spacecraft to enable the MOLA observations we describe in this paper. The outstanding efforts of Ms. Audeliz Matias (Univ. Puerto Rico, Mayaguez) in the correlative analysis of MOLA data with Viking images were essential to the success of this investigation. Motivation for this work has come from Jack Bufton, Jim Abshire, Richard S. Williams Jr., and Richard A. F. Grieve. Helpful discussions with Mike Malin and Jim Head are gratefully acknowledged. Greg Neumann kindly provided rapid access to the nearly 200 MOLA profiles that were analyzed as part of this study. A portion of this research was performed under USRA Contract NAS5-32484. Finally, the senior author (J.B.G) is grateful for the strong support of Cindy, Zachary, and Danica Garvin in making this study possible.

REFERENCES

Barlow, N., and T. Bradley 1990. Martian impact craters: Correlations of ejecta and interior morphologies with diameter, latitude, and terrain. *Icarus* **87**, 156–179.

Clifford, S. M. 1993. A model for the hydrologic and climatic behavior of water on Mars. *J. Geophys. Res.* **98**, 10,973–11,016.

Craddock, R., T. Maxwell, and A. Howard 1997. Crater morphometry and modification in Sinus Sabaeus and Margaritifer Sinus regions of Mars. *J. Geophys. Res.* **102**, 13,321–13,340.

Croft, S. K. 1985. The scaling of complex craters. *Proc. Lunar Planet. Sci. Conf. 15th*, 828–842.

Garvin, J. B. 1996. Topographic characterization and monitoring of volcanoes via aircraft laser altimetry. In *Volcano Instability on the Earth and Other Planets* (W. McGuire, A. Jones, and J. Neuberg, Eds.), Geological Society of London Special Publication No. 110, pp. 137–152. Geological Society of London, London, UK.

Garvin, J. B., and S. Baloga 1999. Inferences on the emplacement dynamics of martian impact crater ejecta: Constraints from MOLA topography. In *Abstracts of the 30th Lunar and Planetary Science Conference.* Lunar and Planetary Institute, Houston, TX. [CD-ROM]

Garvin, J. B., and J. J. Frawley 1998. Geometric properties of martian impact craters: Preliminary results from the Mars Orbiter Laser Altimeter. *Geophys. Res. Lett.* **25**, 4405–4408.

Garvin, J. B., and R. S. Williams, Jr. 1990. Small domes on Venus: Probable analogs of Icelandic lava shields. *Geophy. Res. Lett.* **17**, 1381–1384.

Garvin, J. B., J. J. Frawley, and S. E. H. Sakimoto 1999. North polar dunes on Mars: MOLA measurements and implications for sediment volumes. In *Abstracts of the 30th Lunar and Planetary Science Conference*, Abstract 1721. Lunar and Planetary Institute, Houston, TX. [CD-ROM]

Garvin J. B., S. E. H. Sakimoto, J. J. Frawley, and A. Matias 1998. Martian polar region impact craters: Geometric properties from Mars Orbiter Laser Altimeter (MOLA) observations. In *First International Conference on Mars Polar Science and Exploration*, LPI Contribution 953, pp. 12–13. Lunar and Planetary Institute, Houston, TX.

Garvin, J. B., S. E. H. Sakimoto, C. Schnetzler, and J. J. Frawley 1999. Global geometric properties of martian impact craters: A preliminary assessment using Mars Orbiter Laser Altimeter (MOLA) topography. In *5th International Conference on Mars, Pasadena, CA, July 19–23, 1999*.

Grieve, R. A. F., and M. J. Cintala 1992. An analysis of differential impact melt-crater scaling and implications for the terrestrial impact record. *Meteoritics* **27**, 526–538.

Grieve, R. A. F., and J. B. Garvin 1984. A geometric model for excavation and modification at terrestrial simple impact craters. *J. Geophys. Res.* **89**, 11,561–11,572.

Gudmundsson, M. T. 1989. The Grimsvotn Caldera: Subglacial topography and structure of caldera infill. *Jokull* **39**, 1–21.

Hodges, C. A., and H. J. Moore 1994. *Atlas of Volcanic Landforms on Mars*. USGS Professional Paper 1534. U.S. Govt. Printing Office, Washington, DC.

Howard, A., J. A. Cutts, and K. L. Blasius 1982. Stratigraphic relationships within martian polar cap deposits. *Icarus* **50**, 161–215.

Jankowski, D., and S. Squyres 1993. "Softened" impact craters on Mars: Implications for ground ice and structure of martian regolith. *Icarus* **106**, 365–379.

McGetchin, T., M. Settle, and J. W. Head 1973. Radial thickness variation in impact crater ejecta: Implications for lunar basin deposits. *Earth Planet. Sci. Lett.* **20**, 226–236.

Melosh, H. J. 1989. *Impact Cratering: A Geologic Process*. Oxford, Univ. Press, New York.

Mouginis-Mark, P. J., L. Wilson, and M. T. Zuber 1992. The physical volcanology of Mars. In *Mars* (H. H. Kieffer, B. Jakosky, C. Snyder, and M. Matthews, Eds.), pp. 424–452. Univ. of Arizona Press, Tucson.

Pike, R. J. 1980a. Formation of complex impact craters: Evidence from Mars and other planets. *Icarus* **43**, 1–19.

Pike, R. J. 1980b. *Geometric Interpretation of Lunar Craters*. USGS. Professional Paper 1046-C. USGS, Washington, DC.

Pike, R. J. 1988. Geomorphology of impact craters on Mercury. In *Mercury* (F. Vilas, C. Chapman, M. Matthews, Eds.), pp. 165–273. Univ. of Arizona Press, Tucson.

Plaut, J. J., R. Kahn, E. Guinness, and R. E. Arvidson 1988. Accumulation of sedimentary debris in the south polar region of Mars and implication for climate history. *Icarus* **75**, 357–377.

Roddy, D. J. 1977. Tabular comparison of the Flynn Creek impact crater, United States, Steinheim impact crater, Germany, and Snowball explosion crater, Canada. In *Impact and Explosion Cratering* (D. Roddy, R. Peppin, and R. Merrill, Eds.), pp. 125–162. Pergamon, New York.

Sakimoto, S. E. H., and J. B. Garvin 1999. Topography of impact structures on the north polar cap of Mars. In *Abstracts of the 30th Lunar and Planetary Science Conference*, Abstract 1993. Lunar Planetary Institute, Houston, TX.

Smith, D. E., and 11 colleagues 1998. Topography of northern hemisphere of Mars from the Mars Orbiter Laser Altimeter. *Science* **279**, 1686–1692.

Squyres, S., S. Clifford, R. Kuzmin, J. Zimbelman, and F. Costard 1992. Ice in the martian regolith. In *Mars* (H. H. Kieffer, B. Jakosky, C. Snyder, and M. Matthews, Eds.), pp. 523–556. Univ. of Arizona Press, Tucson.

Strom, R. G., S. Croft, and N. Barlow 1992. The martian impact cratering record. In *Mars* (H. H. Kieffer, B. Jakosky, C. Snyder, and M. Matthews, Eds.), pp. 383–423. Univ. of Arizona Press, Tucson

Thomas, P., S. Squyres, K. Herkenhoff, A. Howard, and B. Murray 1992. Polar deposits of Mars. In *Mars* (H. H. Kieffer, B. Jakosky, C. Snyder, and M. Matthews, Eds.), pp. 767–795. Univ. of Arizona Press, Tucson.

Williams, R. S., Jr., S. Thorarinsson, and E. C. Morris 1983. Geomorphic classification of Icelandic volcanoes. *Jokull* **29**, 29–32.

Wilson, L., and J. W. Head 1994. Mars: Review and analysis of volcanic eruption theory and relationships to observed landforms. *Rev. Geophys.* **32**, 221–264.

Zuber, M. T., and 20 colleagues 1998. Observations of the north polar region of Mars from the Mars Orbiter Laser Altimeter. *Science* **282**, 2053–2060.